Ribosome-binding protein 1, RRBP1, maintains peroxisome biogenesis

Kaneez Fatima[1], Helena Vihinen[2], Bala Ani Akpinar[1], Tamara Somborac[1], Eija Jokitalo[2], Pekka Katajisto[3], Svetlana Konovalova[1]*

[1] Institute of Biotechnology, Helsinki Institute of Life Science (HiLIFE), University of Helsinki, Helsinki, Finland

[2] Electron Microscopy Unit, Institute of Biotechnology, Helsinki Institute of Life Science (HiLIFE), University of Helsinki, Helsinki, Finland

[3] Faculty of Biological and Environmental Sciences, University of Helsinki, Helsinki, Finland

*Corresponding author (svetakonovalova@gmail.com)

Keywords: peroxisome, RRBP1, CRISPR/Cas9, peroxisome biogenesis

ABSTRACT

Peroxisomes are single membrane-bound organelles essential for human health, yet the mechanisms of peroxisome biogenesis are not fully understood. Here using a systematic double screening approach, we identified ribosome-binding protein 1, RRBP1, as a novel peroxisome biogenesis factor in human cells. Deletion of RRBP1 in HEK293T cells led to a reduction in both peroxisome number and peroxisomal protein levels as well as in defects in processing of peroxisomal matrix proteins, such as ACOX1 and thiolase. However, cell proliferation and protein translation were not altered in cells lacking RRBP1. RRBP1 depletion did not affect peroxisome-ER contact sites, and pexophagy did not contribute to the reduction of peroxisomes in RRBP1 KO cells. Instead, in the absence of RRBP1, peroxisomal proteins were processed by proteasomal degradation, suggesting that RRBP1 plays a role in the insertion of these proteins into ER membranes and their stabilization. Altogether our results showed that RRBP1 promotes peroxisome biogenesis in human cells highlighting the power of systematic approaches in discovering novel factors of organellar biogenesis.

INTRODUCTION

Peroxisomes are single membrane-bound organelles, essential for lipid breakdown and β-oxidation of very long-chain fatty acids. Peroxisomes can originate through two distinct mechanisms: *de novo* biogenesis and fission. *De novo* peroxisome biogenesis begins with the assembly of peroxisomal membrane receptors PEX3 and PEX16 at the ER and mitochondria, creating pre-peroxisomal vesicles that fuse. Following fusion, the newly formed peroxisome continues to import peroxisomal membrane proteins via the PEX19-mediated pathway. Once the import machinery is established on the membrane, peroxisomes can import matrix proteins, which are translated on free ribosomes and transported post-translationally from the cytosol. This process leads to the maturation of pre-peroxisomes into fully functional peroxisomes (Sugiura et al., 2017; Kim et al., 2006; Farré et al., 2019; Goldman and Blobel, 1978; Hasan et al., 2013; Rachubinski et al., 1984).

Most of the peroxisomal matrix proteins contain targeting sequences, PTS1 or PTS2, that are recognized by cytosolic peroxins, PEX5 or PEX7 respectively (Walter and Erdmann, 2019; Okumoto et al., 2018; Farré et al., 2019). The translocation of the substrate proteins into the peroxisomal matrix is mediated by factors localized on the peroxisomal membrane such as PEX14, PEX13, and PEX26 (Schliebs et al., 1999; Albertini et al., 1997; Distel et al., 1996; Matsumoto et al., 2003). Although studies in yeast (Akşit and van der Klei, 2018; Erdmann et al., 1989) and mammalian cells (Fang et al., 2004; Fujiki et al., 2014) have identified core components required for peroxisomal matrix import, the discovery of additional factors in recent studies (Baldwin et al., 2021; Guillén-Samander et al., 2021), suggests that more remain to be identified.

To systematically identify factors involved in biogenesis of peroxisomes in mammalian cells we first utilized APEX2-proximity labeling followed by mass spectrometry as a powerful tool to study protein-protein interactions (Lam et al., 2015). Using this approach, we identified factors that specifically interact with peroxisomal matrix cargo. Secondly, we tested these factors by CRISPR-Cas9 KO microscopy screening. Using this double screening approach we revealed ribosome-

binding protein 1, RRBP1, also known as p180/ribosome receptor, as a novel peroxisome biogenesis factor.

Using knockout and knockdown models, we demonstrated that RRBP1 depletion results in peroxisome loss. Notably, RRBP1 KO did not affect cell proliferation or protein translation, and we confirmed that pexophagy was not responsible for peroxisome loss in these cells. Thus, we established that RRBP1 is essential for maintaining peroxisome number in human cells. Although RRBP1 is an ER membrane protein, its depletion did not significantly alter the abundance of the contacts between ER and peroxisomes. However, the inhibition of the proteolytic activity with the proteasome inhibitor MG132, revealed that peroxisomal proteins undergo enhanced proteasomal degradation in RRBP1 KO cells. These findings suggest that RRBP1 is involved in early induction of peroxisome biogenesis by regulating the initial membrane insertion of key peroxisomal components into the ER membrane.

RESULTS

Systematic identification of peroxisome biogenesis factors using a double screening approach

To systematically identify factors required for the protein import into the peroxisomal matrix we first used a proximity-labeling approach followed by mass spectrometry (Lam et al., 2015) (Fig. 1A). Ascorbate peroxidase (APEX2) was fused to ePTS1, the enhanced peroxisomal targeting signal type 1 recognized by PEX5, directing the construct to the peroxisomal matrix. The GFP-APEX2-ePTS1 construct was stably expressed in HEK293T control cells or cells lacking peroxisomes (PEX3 KO or PEX19 KO cells, Supplementary Fig. 1A). The GFP-APEX2-ePTS1 construct is normally recognized by the peroxisomal protein import machinery and delivered to the peroxisomal matrix in control cells. In contrast, in PEX3 KO or PEX19 KO cells that lack peroxisomes, the construct remains in the cytosol (Supplementary Fig. 1B). Under these conditions,

factors involved in recognizing and trafficking ePTS1-containing proteins are expected to accumulate near the GFP-APEX2-ePTS1 construct. Therefore, proteins specifically enriched in proximity to GFP-APEX2-ePTS1 in PEX3 KO or PEX19 KO cells are strong candidates for peroxisome biogenesis factors.

To exclude non-specifically labeled proteins we used parental cells not expressing GFP-APEX2-ePTS1 and cells stably expressing non-targeted GFP-APEX2 as negative control samples.

Biotinylated proteins were extracted from cell lysates using streptavidin beads and analyzed by mass spectrometry. Proteins identified from two replicates for each PEX3 KO and PEX19 KO cells were considered as significant hits. To identify highly specific interactors of GFP-APEX2-ePTS1 in cells lacking peroxisomes we excluded any protein identified in the negative control samples (Supplementary Table 1). Next, we excluded essential proteins (Supplementary Table 2). Following pathway analysis of the remaining candidates, we identified 44 proteins that are potentially involved in peroxisome biogenesis (Fig. 1B, Supplementary Fig. 1 C; Supplementary Table 3). Surprisingly, we did not detect PEX5 among the identified proteins, despite its role as the key factor recognizing PTS1. Notably, PEX5 was not identified as a specific interactor of GFP-APEX2-ePTS1 even in parental cells, suggesting that a combination of technical limitations in the labeling reaction and the unique biological properties of PEX5 may have prevented its detection in the APEX2 proximity labeling assay.

To ensure that only factors with a functional role in peroxisome biogenesis were identified, we performed a secondary CRISPR/Cas9-based microscopy screen of the candidates from the proximity labeling assay (Fig. 1C). For each candidate, two gRNAs were designed and co-transfected with Cas9 into HEK293T cells stably expressing GFP-APEX2-ePTS1, which served as a reporter cell line for peroxisome biogenesis. Live-cell fluorescence microscopy was performed to examine the localization of GFP in the transfected cells, in which redistribution of GFP from peroxisomes to the cytosol indicated disruption of peroxisome biogenesis (Fig. 1C). The phenotype

of the cells was analyzed using live-cell microscopy and the cells were manually classified into four categories based on GFP localization: “no” (GFP localized exclusively to peroxisomes, no mislocalization), “mild” (some mislocalized GFP), “strong” (substantial mislocalized GFP), and “very strong” (extensive mislocalized GFP). Each gRNA was tested in two independent rounds of transfection, with analyses performed at days 7, 10, and 14 post-transfection. As positive controls, gRNAs targeting known peroxisome assembly factors, such as PEX5 and PEX19, produced robust mislocalization of GFP-APEX2-ePTS1 (Fig. 1D,E) without altering its overall expression level (Supplementary Fig. 1E). Among the hits, knockout of ribosome-binding protein 1 (RRBP1) caused strong mislocalization of GFP-APEX2-ePTS1 into the cytoplasm (Fig. 1D, E), suggesting its role in peroxisomal biogenesis.

RRBP1 also known as p180/ribosome receptor, is a transmembrane ER protein. RRBP1 was originally identified as a ribosome receptor for the ER (Savitz and Meyer, 1990) and has also been proposed to regulate local translation in axons (Koppers et al., 2024). Recent studies suggest that RRBP1 plays a role in tethering ER with mitochondria (Anastasia et al., 2021; Cardoen et al., 2024; Hung et al., 2017) and regulates mitophagy (Killackey et al., 2023). However, RRBP1 has not been linked to peroxisomal function previously. Therefore, RRBP1 emerged as a particularly promissing candidate due to its ER localization and established role in ribosome binding and membrane protein translocation – processes closely tied to organelle biogenesis. Together with the strong phenotype observed in our screen (Fig. 1D, E), these features provided the rationale for selecting RRBP1 for detailed functional characterization as a potential peroxisome biogenesis factor.

RRBP1 is required for the maintenance of peroxisome number in human cells

To investigate the involvement of RRBP1 in the maintenance of peroxisomes we generated RRBP1 KO HEK293T clonal cell line expressing the GFP-APEX2-ePTS1 construct by CRISPR/Cas9 gene

editing. To achieve a complete knockout of the RRBP1 gene we used a sgRNA targeting exon 2, common to all isoforms of RRBP1. We confirmed the complete depletion of the RRBP1 protein in the generated RRBP1 KO cell line using immunoblotting (Fig. 2A). We analyzed RRBP1 KO HEK293T cells expressing GFP-APEX2-ePTS1 and its parental cell line as a control. In addition, as positive controls we used cells lacking essential peroxisome biogenesis factors, PEX3 or PEX19, generated in our previous study (Somborac et al., 2023). We observed that the RRBP1 KO cells have significantly less steady-state protein levels of peroxisomal matrix protein, catalase, as well as the peroxisomal membrane proteins, PEX3, PEX19, PEX 14 and PXMP2 compared to the parental cell line (Fig. 2A, B, Supplementary Fig. 3D). In contrast, the protein level of PEX5, an essential peroxisomal matrix protein factor, was induced upon RRBP1 KO (Fig. 2A, B).

Next, we analyzed the peroxisomal function in RRBP1 KO cells by assessing peroxisomal matrix protein import. Although most of the peroxisomal proteins are translated in the cytosol in their mature form, some undergo processing upon import to peroxisomes. Once imported to the peroxisomal matrix, the 72 kDa cytosolic unprocessed acyl-CoA oxidase 1, ACOX1, a PTS1-targeted peroxisomal matrix protein is cleaved into its 50 kDa and 22 kDa mature forms (Kurochkin et al., 2007). Similarly, the 44 kDa unprocessed 3-ketoacyl-CoA thiolase, ACAA1, a PTS2-targeted peroxisomal matrix protein, is processed to 42 kDa upon impot to peroxisomes (Miura et al., 1984). Using immunoblotting we showed that the processing of both ACOX1 and ACAA1, was largely abolished in PEX3 or PEX19 cells lacking peroxisomes (Fig. 2A-C), confirming that this assay can be efficiently used to analyze peroxisomal function as shown previously (Klouwer et al., 2021; Kurochkin et al., 2007). Interestingly, a similar significant decrease in the processing of ACOX1 and ACAA1 was observed in the RRBP1 KO cells (Fig. 2A-C).

Notably, PEX3 or PEX19 KO cells have significantly lower RRBP1 protein levels compared to their parental cells, suggesting that RRBP1 protein is responsive to the absence of peroxisomes. We also observed a slight decrease in the protein levels of the endoplasmic reticulum proteins calnexin

and VAPB in RRBP1 KO cells compared to parental cells (Fig. 2D), suggesting that RRBP1 KO may have a mild impact on the ER. We observed no effect of RRBP1 KO on the steady state level of mitochondrial protein, TOM20 (Fig. 2E), suggesting that mitochondrial mass is not affected in cells lacking RRBP1.

To validate our findings on RRBP1 KO cells we performed transient knock down of RRBP1 using endoribonuclease-prepared short interfering RNA (esiRNA) in HEK293T cells stably expressing GFP-APEX2-ePTS1. GFP esiRNA was used as a negative control while esiRNA targeting a peroxisomal import factor essential for the assembly of functional peroxisomes, PEX5, was used as a positive control. In cells silenced for RRBP1, protein levels of ACAA1 and catalase were reduced (Fig. 3A, B, D) and the processing of ACOX1 was significantly decreased similar to PEX5 silencing (Fig. 3C). Importantly, similar to RRBP1 KO cells we showed mislocalization of GFP-APEX2-ePTS1 construct to the cytosol in cells acutely silenced for RRBP1 (Fig. 3E).

Thus, we demonstrated that loss of RRBP1 leads to peroxisomal deficiency, indicating that RRBP1 plays a specific role in peroxisome maintenance.

RRBP1 KO causes a decreased number of peroxisomes in human cells

Next, we investigated whether the peroxisome number is affected by the loss of RRBP1. We used RRBP1 KO HEK293T cells stably expressing GFP-APEX2-ePTS1 and its parental cell line as a negative control. Live-cell fluorescence microscopy confirmed the absence of RRBP1 in KO cells and revealed a reduced number of GFP-positive puncta representing mature peroxisomes compared to the parental cells (Supplementary Fig. 1G). In addition, GFP-APEX2-ePTS1 was partially localized to cytosol in cells lacking RRBP1, while in parental HEK293T cells the construct was correctly localized to peroxisomes, confirming our result from the CRISPR screen (Fig. 1D). These

data collectively show that the import of peroxisomal matrix proteins is compromised in RRBP1 KO.

To study if RRBP1 KO also affects peroxisome number, we performed high-resolution immunofluorescence confocal microscopy of RRBP1 KO cells using PMP70 and PEX14 as a membrane markers and catalase as a matrix marker of peroxisomal structures. As a positive control we used PEX3 KO or PEX19 KO HEK293T cells lacking peroxisomes. The number of PMP70-, PEX14- or catalase-positive structures per cell were reduced in RRBP1 KO cells compared to the parental cells (Fig. 4 A-E), confirming that RRBP1 is required for maintaining peroxisome number. Notably, cell volume was unaffected by RRBP1 KO, excluding this as a factor contributing to the reduced peroxisome abundance (Fig. 4F).

Altogether these results show that RRBP1 is an important factor involved in the maintenance of peroxisome number in human cells.

RRBP1 does not localize to peroxisomes

Our data indicate that RRBP1 maintains peroxisome biogenesis. Previously, RRBP1 was described as an ER transmembrane protein (Shibata et al., 2010; Ogawa-Goto et al., 2007; Savitz and Meyer, 1990). Thus, the role of RRBP1 in peroxisome biogenesis could be mediated through the ER. To analyze whether in addition to ER, RRBP1 is localized to peroxisomes we performed colocalization analysis using confocal microscopy and corresponding antibodies labeling peroxisomes, ER, or mitochondria (Fig. 5A). RRBP1 mainly localized to ER (overlay of RRBP1 with calnexin) and showed some localization to mitochondria (ATPIF1 colocalization with RRBP1), while we observe only weak colocalization of RRBP1 with peroxisomes (catalase with RRBP1) (Fig. 5A, B).

To further confirm that RRBP1 does not localize to peroxisomes, we examined RRBP1 protein in isolated peroxisomes using immunoprecipitation (IP) as described by Ray et al. (Ray et al., 2020).

We generated clonal HEK293T cell lines stably expressing 3×HA-EGFP-PEX26 at either low or high levels and verified peroxisomal localization of tagged PEX26 by confocal microscopy (Supplementary Fig. 2A,B). The IP procedure yielded highly purified peroxisomes, confirmed by the absence of ER (calnexin) and cytosolic (GAPDH) contamination (Fig. 5C). Importantly, RRBP1 was not detected in the peroxisomal fraction (Fig. 5C). These results demonstrate that RRBP1 does not localize to peroxisomes, instead its role in peroxisome biogenesis is mediated at the ER.

Thus, our data clearly show that RRBP1 does not localize to peroxisomes, instead its role in peroxisome biogenesis is mediated at the level of ER.

RRBP1 KO causes peroxisomal deficiency independent of ER stress

Since RRBP1 is an ER protein that may influence protein translation and cell proliferation, we tested whether RRBP1 KO cells exhibited altered proliferation. RRBP1 KO did not affect cell proliferation (Supplementary Fig. 2A), and the protein translation rate measured by puromycin incorporation into a newly synthesized proteins also remained unchanged (Supplementary Fig. 2B,C). However, we observed a reduction in specific ER proteins, including VAPB, calnexin, IRE1α, and BiP, in RRBP1 KO cells compared to the parental cell line (Supplementary Fig. 2D,E; Fig.2A,D). This suggests a mild disruption of ER homeostasis. However, the levels of SEC61 and RPL7 were unaltered indicating that the overall machinery for protein synthesis and translocation as well as ribosomal assembly remains unaffected.

Peroxisome-ER contact sites are not affected in RRBP1-depleted cells

Recent studies suggest that RRBP1 can act as a tether in contact sites between ER and mitochondrial membranes ensuring metabolic communication between two organelles (Hung et al.,

2017; Anastasia et al., 2021). To test whether RRBP1 has a role in maintaining peroxisome-ER contacts we used electron microscopy. We took advantage of APEX2, a well-characterized powerful tool for labeling intracellular structures in electron microscopy studies (Martell et al., 2017; Rae et al., 2021; Sengupta et al., 2019; Lam et al., 2014). Using DAB staining we labeled peroxisomes in RRBP1 KO HEK293T cells stably expressing GFP-APEX2-ePTS1 and its parental cell line. We observed that neither RRBP1 silencing by siRNA nor RRBP1 KO affected the number of contact sites between the ER and peroxisomes (Fig. 6A-E). Additionally, electron microscopy analysis of peroxisomal morphology in RRBP1 KO cells revealed no changes in peroxisomal size or shape (Fig. 6F, G).

The decreased number of peroxisomes in RRBP1 KO cells is independent of pexophagy but associated with increased proteasomal degradation of peroxisomal membrane proteins.

We showed that the steady state number of peroxisomes is decreased upon RRBP1 KO (Fig. 4A-E). Peroxisomal homeostasis is regulated by the interplay between peroxisome biogenesis and selective autophagy of peroxisomes, pexophagy (Demers et al., 2023; Germain and Kim, 2020; Sakai et al., 2006). Therefore, the decreased peroxisome number upon RRBP1 KO could be the result of affected peroxisome biogenesis where less peroxisomes were formed or induced pexophagy leading to the loss of peroxisomes. To distinguish between these two possibilities, we tested whether pexophagy is induced in RRBP1 KO cells. First, we assessed the steady-state levels of autophagy markers in RRBP1 KO cells and observed a reduction in LC3B and ATG5 levels compared to the parental cell line (Fig. 7A, B). However, steady-state levels of autophagy markers such as LC3B or ATG5 cannot reliably measure autophagic activity, since autophagy is a dynamic process in which intermediates are continuously generated and degraded. For this reason, we used chloroquine to inhibit pexophagy and assessed whether blocking pexophagy could restore the levels of peroxisomal proteins in RRBP1 KO cells. We confirmed the inhibition of autophagy upon

chloroquine treatment by induction of LC3B-II, indicating the accumulation of autophagosomes (Fig. 7A, B). However, chloroquine treatment did not rescue the levels of PEX3 or PMP70 proteins in RRBP1 KO cells (Fig. 7A, B). These results conclusively suggest that pexophagy is not induced in RRBP1 knockout cells. Consequently, the reduced number of peroxisomes in cells lacking RRBP1 is likely due to its involvement in peroxisome biogenesis.

To investigate whether peroxisomal proteins undergo proteasomal degradation in the absence of RRBP1, we inhibited the proteasomal degradation pathway using MG132 treatment. Our results revealed that PEX3 and PEX16 were significantly restored in RRBP1 KO cells upon MG132 treatment (Fig 7C, D), suggesting that their reduction in RRBP1 KO cells is due to proteasomal degradation. Since both PEX3 and PEX16 play crucial roles in initiating peroxisome *de novo* biogenesis via the ER (Aranovich et al., 2014; Kim et al., 2006), their recovery upon proteasomal inhibition indicates that RRBP1 may be involved in the insertion of these proteins into ER membranes. Furthermore, in the parental cell line, MG132 treatment resulted in a significant induction of RRBP1, suggesting that RRBP1 itself has a high turnover rate and may be subject to proteasomal degradation.

These findings highlight a potential regulatory mechanism in which RRBP1 helps maintain peroxisomal membrane protein stability, and its absence leads to increased degradation of key peroxisome biogenesis factors.

DISCUSSION

In this study, we identified and characterized RRBP1 (also known as p180/ribosome receptor), an ER transmembrane protein, as a novel factor involved in peroxisome biogenesis. RRBP1 has been previously implicated in ribosome binding (Savitz and Meyer, 1990), ER-mitochondria tethering (Anastasia et al., 2021; Hung et al., 2017; Cardoen et al., 2024), mitophagy regulation (Killackey et

al., 2023), and local axonal translation (Koppers et al., 2024) but its role in peroxisomal function has not been identified.

We showed that cells lacking RRBP1 lose peroxisomes. However, in contrast to cells lacking known essential components of peroxisome biogenesis machinery, like PEX3 and PEX19, RRBP1 KO did not result in complete absence of peroxisomes, indicating that although RRBP1 plays a role in peroxisome biogenesis it is not an essential factor.

Interestingly, in RRBP1 KO cells as well as in the PEX3 or PEX19 KO cells completely lacking peroxisomes, we observed induction of PEX5 protein level, a cytosolic peroxin essential for protein delivery into the peroxisomal matrix. These data indicate a complex role for RRBP1 in peroxisomal protein homeostasis. Notably, in cells lacking peroxisomes PEX3 KO or PEX19 KO cells, the RRBP1 protein level was reduced, suggesting that RRBP1 is responsive to the absence of peroxisomes.

To determine whether peroxisome loss in RRBP1 KO cells was due to enhanced peroxisomal degradation, we tested whether blocking pexophagy could restore peroxisomal protein levels. However, inhibition of pexophagy did not rescue peroxisomal protein levels in RRBP1 KO cells. Interestingly, we observed a significant reduction in steady-state LC3B levels in RRBP1 KO cells, which remained lower than in treated parental cells even after pexophagy inhibition. These findings suggest that pexophagy does not contribute to peroxisome loss in RRBP1 KO cells. Instead, the reduced pexophagy rate in RRBP1 KO cells is likely a consequence of the overall decrease in peroxisome abundance.

It is interesting to show that peroxisome biogenesis in human cells requires RRBP1, an ER membrane protein. Notably, RRBP1 KO did not affect cell proliferation or protein translation. Moreover, SEC61 and RPL7 remained unchanged in cells lacking RRBP1, suggesting that RRBP1 does not affect translation or translocation machinery.

The classical model of peroxisome biogenesis suggests that peroxisomal membranes originate from ER in the form of budding pre-peroxisomal vesicles (Lam et al., 2010). However, our APEX2-based proximity labeling suggests that RRBP1 interacts with cargo proteins containing PTS1 peroxisomal targeting signal, proposing that RRBP1 has a role in the import of peroxisomal matrix proteins. Importantly, in contrast to peroxisomal membrane proteins, peroxisomal matrix proteins are not detected in ER (Geuze et al., 2003; Van Der Zand et al., 2010). We also showed that RRBP1 is not localized to peroxisomes, thus making it unlikely that RRBP1 is directly involved in peroxisomal protein import. Instead, our data suggest that RRBP1 may play an indirect role by facilitating the recruitment of other factors to peroxisomal membranes that are required for matrix protein import.

How can an ER protein be involved in peroxisome biogenesis? Recent studies indicate that peroxisomes interact closely with the ER through membrane contact sites, which are crucial for peroxisome dynamics, biogenesis, and metabolic signaling (Costello et al., 2017; Hua et al., 2017; Guillén-Samander et al., 2021; Baldwin et al., 2021). However, we did not observe significant changes in the abundance of peroxisome-ER contact sites in RRBP1-depleted cells. However, it is important to note that the DAB staining method used in our study detects only mature peroxisomes, therefore, our data cannot exclude a potential role of RRBP1 in regulating contacts between the ER and pre-peroxisomes.

Our findings indicate a reduction in both peroxisomal membrane and matrix proteins, along with a decreased peroxisome number, suggesting a potential disruption in *de novo* peroxisome biogenesis. We demonstrated that the decreased levels of peroxisomal proteins, such as PEX3 and PEX16, in RRBP1 KO cells result from enhanced proteasomal degradation. Therefore, a potential mechanism by which RRBP1 contributes to peroxisome biogenesis is through the integration of PEX16 into the ER membrane and its stabilization. PEX16 is known to initiate peroxisome formation by recruiting peroxisomal membrane proteins.

Previous studies have shown that RRBP1 promotes the localization of specific mRNAs to the ER surface (Koppers et al., 2024; Cui et al., 2012; Cui and Palazzo, 2014) and a number of mRNAs encoding peroxisomal proteins are enriched on the ER (Haimovich et al., 2016). Additional evidence indicates that targeted mRNA trafficking and local translation contribute to peroxisome biogenesis (Dahan et al., 2022; Zipor et al., 2009). Taken together, these findings support the idea that RRBP1 facilitates the efficient translation of critical peroxisomal proteins, such as PEX16, by directing their mRNAs to the ER. However, the precise mechanism remains unclear whether RRBP1 directly assists in the insertion of peroxisomal proteins or indirectly regulates their recruitment by influencing mRNA localization.

Interestingly, RRBP1 appears to be a metazoan-specific protein, its homologs are not found in yeast. Therefore, despite the conservation of general protein targeting mechanisms in eukaryotic cells, the role of RRBP1 in peroxisome biogenesis can represent a specific pathway of peroxisomal maintenance in higher eukaryotes.

In conclusion, the identification and characterization of RRBP1 as a factor involved in peroxisomal formation advances our understanding of organelle biogenesis, a complex process involving multiple steps and diverse intracellular cooperation.

MATERIALS AND METHODS

Cell culture

HEK293T cells (ATCC, CRL-11268) were cultured (37°C, 5% CO2) in DMEM (Pan-Biotech, P04-03600) supplemented with 10% fetal bovine serum (GIBCO, 10270106), l-glutamine (GIBCO, 25030081) and penicillin/streptomycin (GIBCO, 15140122). The cells were regularly tested for mycoplasma contamination. TransIT-X2 (MirusBio, MIR 6000) or TransIT2020 (Mirus, MIR 5400) were used for cell transfection according to manufacturer's instruction.

Generation of knockout cell lines

PEX3 KO and PEX19 KO HEK293T cells were generated in our previous study (Somborac et al., 2023) using CRISPR/Cas9 genome editing. Cells were co-transfected with two gRNAs and pSpCas9n(BB)-2A-Puro (PX462) V2.0 (Addgene, 62987 (Ran et al., 2013)). PEX3 gRNAs were ACGTGCTTGAAAGGGGGCAT and CACCTCCAAGGACCGTGCCC. PEX19 gRNA were GGGCCCCAGAAGAGATCGCC and GGGGCCGTGGTGGTAGAAGG. After 24 h the cells were selected with puromycin and expanded. T7 assay was used to confirm genome editing. Single cell clones were obtained and validated using immunoblotting analysis.

To generate RRBP1 KO HEK293T cells expressing EGFP-FLAG-APEX2-ePTS1 single gRNA transcriptional cassette prepared by PCR and pCAS9-mCherry empty (Addgene, 80975 (Schmid-Burgk et al., 2016)) were co-transfected into HEK293T cells expressing EGFP-FLAG-APEX2-ePTS1. After 24 h of transfection mCherry-positive cells were sorted by FACS onto 96-well plate containing DMEM media supplemented with 15% fetal bovine serum (GIBCO, 10270106), l-glutamine (GIBCO, 25030081) and penicillin/streptomycin (GIBCO, 15140122) and single cell clones generated. The RRBP1 KO cells were validated using immunoblotting analysis. Exon 1 in

RRBP1 is non-coding, therefore we used gRNA targeting the first coding exon common to all isoforms of RRBP1, exon 2. The sequence of sgRNA was CGAAGGAGGACAGTCACATT.

Plasmid construction

To generate GFP-APEX2-ePTS1 (pLL3.7-GFP-FLAG-APEX2-ePTS1) we used PCR overlap extension. FLAG-APEX2 fragment was amplified form pcDNA3 APEX2-NES (Addgene, 49386 (Lam et al., 2015)), ePTS1 was generated using corresponding primers. The resulting fused construct was inserted into pLL3.7 vector (11795 (Rubinson et al., 2003)) using EcoRI and NheI restriction sites. To generate GFP-APEX2 (pLL3.7-GFP-FLAG-APEX2) GFP-FLAG-APEX2 fragment was amplified from pLL3.7-GFP-FLAG-APEX2-ePTS1 plasmid and ligated into pLL3.7 vector. All plasmids were confirmed by Sanger sequencing. Primers used for the cloning are in Supplementary Table 4.

Stable cell line generation

HEK293T stably expressing GFP-APEX2-ePTS1 or GFP-APEX2 were generated by using standard lentiviral cell line generation protocol. Briefly, WT, PEX3 KO or PEX19 KO cells were co-transfected with pMD2.G (Addgene, 12259), psPAX2 (Addgene,12260) and pLL3.7-GFP-FLAG-APEX2-ePTS1 or pLL3.7-GFP-FLAG-APEX2 using TransIT-2020 (MirusBio, MIR 5400) following manufacturer's instructions. Single cell clones were obtained by FACS. The expression of the constructs was confirmed by immunoblotting.

To generate HEK293T cells stably expressing HA-PEROXO (3xHA-EGFP-PEX26) the cells were co-transfected with lentiviral construct pLJC5-3XHA-EGFP-PEX26 (Addgene, 139054; Ray et al., 2020), together with pMD2.G (Addgene, 12259) and psPAX2 (Addgene,12260) using TransIT-

2020 (MirusBio, MIR 5400) following manufacturer's instructions. Cell populations with low or high GFP expression were subsequently isolated by FACS to establish cell lines.

APEX2-proximity labeling

APEX2-proximity labeling was performed using previously described protocol (Hung et al., 2016) with few modifications. HEK293T cells were grown on T75 flasks. The media was changes and 500 µM biotin-phenol was added to the cell culture media for 30 min (37°C, 5% CO2). Proximity labeling was induced by adding 10 mM of H_2O_2 (Fisher Scientific, BP2633-500). The reaction was stopped after 1 min, by removing the media and washing the cells with quencher solution (10 mM sodium ascorbate, 5 mM Trolox and 10 mM sodium azide solution in PBS). Cells were collected in 15 mL quencher solution and pelleted at 3 000 g at 4 °C for 10 min. Cell pellets were flash frozen in liquid nitrogen. When processing all cell lines was complete, pellets were lysed in RIPA lysis buffer supplemented with protease inhibitor cocktail (Thermo Scientific, 10320015), 1 mM PMSF, 5 mM Trolox, 10 mM sodium azide and 10 mM sodium ascorbate. Cell lysates were incubated on ice for about 2 min and then centrifuged at 15 000 g at 4 °C for 10 min. Streptavidin magnetic beads (Thermo Scientific, 88816) were washed twice with RIPA lysis buffer supplemented with protease inhibitor cocktail (Thermo Scientific, 10320015), 1 mM PMSF, 5 mM Trolox, 10 mM sodium azide and 10 mM sodium ascorbate. Then, clarified cell lysates were added to the beads and incubated overnight with rotation at 4 °C. Biotinylated proteins were eluted by boiling the beads in elution buffer (3× protein loading buffer supplemented with 2 mM biotin and 20 mM DTT) for 10 min. Tubes were briefly centrifuged and using a magnetic rack, samples were collected, flash frozen in liquid nitrogen and stored at -80 °C.

Frozen eluates were thawed on ice and run on 10% separating gel at 200 V for 9 min. Samples were cut from the gel, stained with Coomassie, and washed twice with H_2O. Then individual lanes were

cut out and stored at -20 °C in separate microfuge tubes. Scalpels used to cut the gel were single use, and the samples were loaded with one empty well between.

Mass spectrometry analysis of proteins

Protein bands were cut out of the SDS-PAGE gel and "in-gel" digested. Cystein bonds were reduced with 0.045M dithiothreitol (Sigma-Aldrich, D0632) for 20 min at 37 °C and alkylated with 0.1 M iodoacetamide (Fluka, Sigma-Aldrich, 57670) at room temperature in the dark for 30 min. Proteins were digested with 0.75 µg trypsin (Sequencing Grade Modified Trypsin, V5111, Promega) overnight at 37 °C. After digestion, peptides were purified with C-18 Micro SpinColumns (The Nest Group Inc. USA) according to manufacturer's instructions. The dried peptides were reconstituted in 30 µl 0.1% trifluoroacetic acid (TFA) and 1% acetonitrile (ACN) in LC-MS grade water. The mass spectrometry analysis was performed on an Orbitrap Elite and Q Exactive ESI-quadrupole-orbitrap mass spectrometer coupled to an EASY-nLC 1000 nanoflow LC (Thermo Fisher Scientific), using the Xcalibur version 3.1.66.10 (Thermo Scientific) as described in (Liu et al., 2018). Acquired spectral data files were searched against the human component of UniProtKB/SwissProt database using SEQUEST search engine in the Proteome Discoverer 1.4 (Thermo Scientific). The following parameters were applied: only fully tryptic peptides were allowed with maximum of two missed cleavages, precursor mass tolerance and fragment mass tolerance were set to ±15 ppm and 0.05 Da, respectively. Carbamidomethylation of cysteine was defined as static modification and oxidation of methionine was set as variable modification.
The mass spectrometry data were filtered and presented as peptide spectrum matches.

esiRNA gene silencing

HEK293T cells expressing EGFP-FLAG-APEX2-ePTS1 were plated in 6-well plate 24 h before transfection. The cells were transfected with 25 nM esiRNA targeting GFP (Merck, EHUEGFP),

RRBP1 (Merck, EHU073471), or PEX5 (Merck, EHU090061) using TransIT-X2 (MirusBio, MIR 6000). After 72 h the cells were collected for immunoblotting analysis.

For electron microscopy, HEK293T cells expressing EGFP-FLAG-APEX2-ePTS1 were plated in 6-well plate containing small 13 mm glass coverslips 24 h before transfection. The cells were transfected with 25 nM esiRNA targeting LUC (Merck, EHURLUC) or RRBP1 (Merck, EHU073471), using FuGENE® HD Transfection reagent (Promega, cat#E2311). After 72 h the coverslips were fixed, and samples were prepared for electron microscopic analysis. The esiRNA cDNA target sequences are in the Supplementary Table 5.

CRISPR/Cas9 microscopy screen

To perform CRISPR/Cas9 microscopy screen for each 44 selected candidates and two positive controls (PEX5 and PEX19) two gRNAs were designed, except for CSK21, for which only one target sequence was found with sufficient specificity. gRNAs with U6 overhang at 5' and terminator overhang at 3' were purchased as oligos (Supplementary Table 6). U6 was cloned from PX335-dCas9-VP192-PGKpuro using PCR. Obtained U6 was 5'-tailed and amplified using PCR. 3'-tailed terminator was generated using PCR. gRNA transcriptional cassette was generated by PCR using 5'-tailed U6, 3'-tailed terminator, and U6 overhang-gRNA-terminator overhang as described and utilized in (Balboa et al., 2015; Konovalova et al., 2023, 2018). The sequences of used oligos are in Supplementary Table 4.

HEK293T cells expressing EGFP-FLAG-APEX2-ePTS1 were plated in 24-well plates 24 h before the transfection. The cells were co-transfected with a single gRNA and pCAS9-mCherry empty (Addgene, 80975 (Schmid-Burgk et al., 2016)) using TransIT-2020 (Mirus, MIR 5400). The cells were passaged when needed. Two rounds of transfections were performed for each gRNA, each time the cells were analyzed three times at 7, 10, and 14 post-transfection days using EVOS FLoid Imaging System (Thermo Fisher Scientific). The phenotype of the cells was manually classified

based on GFP localization: “no” (GFP localized exclusively to peroxisomes, no mislocalization), “mild” (some mislocalized GFP), “strong” (substantial mislocalized GFP), and “very strong” (extensive mislocalized GFP). The investigator was blinded to the group allocation during the cell analysis.

Live-cell fluorescence microscopy

Live microscopy imaging was performed on cells in 6-weel or 24-well plates using EVOS FLoid Imaging System (Thermo Fisher Scientific) equipped with 20x objective or Eclipse TS100 (Nikon) equipped with 40× objective.

Western blotting

HEK293T cells were lysed in RIPA buffer (Cell Signaling, 9806S) supplemented with protease inhibitor cocktail (Thermo Scientific, 78429). Following 15 min incubation on ice, the samples were centrifuged at 14 000 g for 10 minutes at +4°C. Protein concentration was measured by bicinchoninic acid (BCA) assay (Thermo Fisher, 23228). Protein lysates were supplemented with a laemmli sample buffer (60 mM Tris-Cl pH 6.8, 2% SDS, 10% glycerol, 5% β-mercaptoethanol, 0.01% bromophenol blue), boiled for 5 min at 95° and resolved on 10 % or 7.5 % Mini-PROTEAN TGX Precast Gels (Bio-Rad, 4561033, 4561036, 4561023, 4561026). The SDS-PAGE was performed at 100 V for 5 min and then 120 V for 1 h 15 min using SDS running buffer (30 g Tris, 144 g glycine, 10 g SDS to 1 L distilled water). Then the proteins were transferred to a 0.2-µM PVDF membrane (Bio-Rad, 1704150) by Trans-Blot Turbo Transfer System (Bio-Rad) using pre-installed settings (2.5 A for 7 min) for transferring proteins of mix molecular weight. The membranes were blocked in 5% milk or 5% BSA in TBST (TBS–Tween 20 (0.1%)) for 1 h at room temperature. Proteins were immunoblotted with the indicated primary antibodies in TBS–Tween 20 (0.1%) containing 1% or 5% BSA for overnight, at +4 °C. Following primary antibodies were used:

anti-catalase, 1:1000 (CST, 12980S); anti-RRBP1, 1:1000 (Proteintech, 22015-1-AP); anti-PEX3, 1:1000 (Schmidt et al., 2012); anti-PEX14, 1:1000 (Abcam, 183885); anti-PEX16, 1:1000 (Proteintech, 14816-1-AP); anti-Pex5, 1:1000 (Invitrogen, PA5-58717); anti-calnexin, 1:1000 (Abcam, 22595); anti-PMP70, 1:800 (Sigma, SAB4200181); anti-GFP, 1:1000 (Aves, GFP-1020); anti-TOM20, 1:500 (CST, 42406); anti-ACOX1, 1:1000 (Proteintech, 10957-1-AP); Anti-ACAA1, 1:2000 (Sigma-MERCK, HPA007244); anti-acetylated tubulin, 1:1000 (Sigma-MERCK, T7451); anti-GAPDH, 1:10000 (Sigma-MERCK, G9545); anti-ATG5, 1:2500 (Proteintech, 10181-2-AP); anti-LC3B 1:1000 (Novus biologicals, 600-1384); anti-VAPB, 1:5000 (Proteintech, 14477-1-AP); anti- BiP 1:1000 (CST, 3177); anti- IRE1α 1:1000 (CST, 3294); anti- SEC61A 1:1000 (Abcam, 183046); anti-puromycin antibody 1:10000 (Sigma, MABE343). Next, the membranes were washed with TBST quickly three times and then three times for 15 min at room temperature on shaker. Then the membranes were incubated with HRP conjugated secondary antibodies against mouse 1:5000 (CST 7076S), rabbit (CST 7074S) or chicken (Promega G135A) in TBST containing 1% BSA for 1 h at room temperature on shaker. Then the membranes were washed with TBST quickly three times and then three times for 15 min at room temperature on shocker. ECL western blotting substrate (Thermo Scientific, 32106) was applied to the membrane and chemiluminescence was captured by Chemidoc imaging system (Bio-Rad). Quantification of the bands was performed by Image Lab Software (Bio-Rad).

Immunofluorescence

HEK293T were cultured on 13-mm coverslips 24 h before fixation. Then the media was removed, and the cells were washed three times with PBS. The cells were fixed with 4% paraformaldehyde for 10 min at room temperature and washed three times with PBS. Then the cells were permeabilized with 0.2% Triton X-100 in PBS for 15 min at room temperature and washed with PBS. Next DAPI (1:1000 in PBS) was added for 10 min at room temperature. The cells were

washed with PBST (0.1% Tween 20 in PBS) and blocked with 5% BSA in PBST for 2 h at room temperature. The cells were then incubated with corresponding primary antibodies diluted in 5% BSA in PBST overnight at +4 ºC. Following primary antibodies were used: anti-catalase, 1:400 (CST, 12980S); anti-RRBP1, 1:500 (GeneTex GT5610); anti-calnexin, 1:1000 (Abcam, 22595); anti-PEX14, 1:250 (Abcam, 183885); anti-PMP70, 1:150 (Sigma, SAB4200181); anti-GFP, 1:10000 (Aves, GFP-1020); anti-TOM20, 1:250 (CST, 42406); anti-ATPIF, 1:100 (CST 8528). Then the cells were washed with PBST three times for 15 min. The cells were incubated with secondary antibodies diluted 1:1000 in 5% BSA in PBST (anti-mouse Alexa Fluor 555, CST 4409S; anti-mouse Alexa Fluor 647, Invitrogen, A-21235; anti-rabbit Alexa Fluor 555, CST, 4413S; anti-rabbit Alexa Fluor 647, CST, 4414S; anti-chicken Alexa Fluor 488, Invitrogen, A-11039) for 1 h at room temperature and washed with PBST three times for 5 min. Finally, the cells were mounted using antifade mounting media (Vector Laboratories, H-1700-10). The slides were left to dry overnight at room temperature and then stored at +4 ºC until analysis. The cells were imaged using upright SP8 confocal microscope (Leica).

Quantitative analysis of immunofluorescence images

Imaris Software was used for the analysis of confocal immunofluorescence images. For colocalization analysis Coloc tool within the Surpass system (version 9.5.1) was used. The images were carefully adjusted manually to distinguish between background and signal. The Mander's overlap coefficient was used to quantify the percentage of overlap. In each sample, 5-8 fields of view were analyzed, with each field capturing around 60-120 cells.

To quantify PMP70-, PEX14- or catalase-positive dots, counting cell number or volume, the confocal microscopy images were processed and reconstructed in 3D model using Imaris software. PMP70-, PEX14- or catalase-positive dots were counted using "Dots" function. PMP70, PEX14 or catalase signal was adjusted for the optimal dot detection: X4 diameter (0.5) and model PSF (1.5).

The number of PMP70-, PEX14- or catalase-positive dots was normalized to the number of the cells in the specific field of view.

The cell number was counted based on DAPI nuclear staining. Parameters were set with an XY diameter of 7 to optimize nucleus detection. To analyze the cell volume, PMP70, PEX14 or catalase signal was adjusted to cover the cytosolic area and eliminate any redundant covered regions and debris. Within the Surpass system, a surface was added with default settings, excluding the shortest distance calculations.

Peroxisome isolation by PEROXO-Tag IP

Peroxisomes were isolated as described by (Ray et al., 2020) with slight modifications. HEK293T cells stably expressing 3×HA-EGFP-PEX26 were cultured in two 10-cm dishes for 24 h. Plates were placed on ice and washed twice with cold PBS, after which cells were scraped into 1 ml cold KPBS and pelleted at 1,000 × g for 2 min at 4 °C. Pellets were resuspended in 1 ml KPBS. For whole-cell lysates, 5 µl of the resuspended pellet was mixed with 50 µl NP-40 lysis buffer containing protease inhibitors. The remaining 995 µl was homogenized on ice using a 2-ml Dounce homogenizer (25 strokes). The homogenate was centrifuged at 1,000 × g for 2 min at 4 °C, and the supernatant was collected. The supernatant was incubated with 200 µl anti-HA magnetic beads (Pierce Anti-HA Magnetic Beads, Thermo Scientific, Cat. #88836) on a rotator at 4 °C for 3.5 min. Beads were washed 10 times with cold KPBS, with tubes replaced after the first and final washes. Beads were resuspended in 50 µl NP-40 lysis buffer containing protease inhibitors, incubated on ice for 10 min, and removed using a magnetic stand. The supernatant was centrifuged at 21,000 × g for 10 min at 4 °C, and the resulting clarified fraction was collected as the purified peroxisome protein sample. Prior to immunoblot analysis, both whole-cell lysates and purified peroxisomes were sonicated in a water bath sonicator for three 30-s cycles. Protein concentrations were determined by BCA assay, and proteins were analyzed by western blotting.

Pexophagy assay

RRBP1 KO HEK293T cells expressing EGFP-FLAG-APEX2-ePTS1 or parental cell line were plated on 6-well plate 24 h before the treatment. 100 µM chloroquine was added to the cells cultured in complete DMEM media. The cells were incubated for 3 h, after the incubation the cells were collected and used for western blotting analysis.

Proteosomal inhibition assay

Parental cell line or RRBP1 KO HEK293T cells expressing EGFP-FLAG-APEX2-ePTS1 were plated on 12-well plate 24 h before the treatment. The cells were treated with 10 µM MG132 for 4 h, then the cells were collected and used for western blotting analysis.

Translation assay

Protein translation rate was analyzed by SUrface SEnsing of Translation (SUnSET) method which involves puromycin labeling of nascent proteins followed by immunoblotting to detect the labeled proteins (Schmidt et al., 2009). HEK293T cells expressing EGFP-FLAG-APEX2-ePTS1 or RRBP1 KO HEK293T cells expressing EGFP-FLAG-APEX2-ePTS1 were plated in 12 well plate. After 24 h, both set of cells were treated with 10 µg/ml puromycin and incubated for 20 min in 37°C, 5% CO2 incubator. Afterwards, the cells were collected and lysed, followed by immunoblot analysis.

Cell proliferation assay

HEK293T, HEK293T cells expressing EGFP-FLAG-APEX2-ePTS1 or RRBP1 KO HEK293T cells expressing EGFP-FLAG-APEX2-ePTS1 were plated in 48-well plate at a starting density of 23,000 cells per well. After 24 h, the cells were resuspended and mixed with trypan blue stain (1:1). Cell counting was performed using the Bio-Rad TC20 automated cell counter.

Transmission electron microscopy

RRBP1 KO HEK293T cells expressing EGFP-FLAG-APEX2-ePTS1 or parental cell line were grown on glass coverslips (thickness #1) and fixed with 2% glutaraldehyde (EM-grade) in 0.1 M sodium cacodylate buffer, pH 7.4, supplemented with 2 mM $CaCl_2$. After fixation for 30 min, at RT, the samples were washed with sodium cacodylate buffer followed by washing with 50 mM glysine-sodium hydroxide buffer, pH 10.5. For identification of peroxisomes, the cells expressing APEX2 were labelled with 5 mM 3,3'-diaminobenzidine (DAB) and 0.15% H_2O_2 in glycine-sodium hydroxide buffer for 20 -25 min, on ice, in dark. The reaction was stopped by washing the samples with glycine-sodium hydroxide buffer which after the cells were postfixed with 1% reduced osmium tetroxide in 0.1 M sodium cacodylate buffer for 1 h, on ice. After washing the samples were gradually dehydrated in ethanol and acetone prior flat embedding (Jokitalo et al., 2001) in epoxy (TAAB 812, Aldermaston, UK). Sections of 60 nm were cut using an Ultracut UC7 ultramicrotome (Leica, Vienna, Austria), post-stained with uranyl acetate and lead citrate, and examined at 100 kV using an HT7800 transmission electron microscope (Hitachi High-Technologies, Tokyo, Japan). Images were acquired using a Rio9 CMOS-camera (AMETEK Gatan Inc., Pleasanton, CA).

PO-ER contact site analysis

Three independent experiments were performed. In each experiment for each cell line 13-18 cells having peroxisomal profiles were selected using systematic random sampling for the analysis of peroxisomes and peroxisome-ER contact sites. All the peroxisomes in the selected cells (n = 437 for the parental cell line, n = 403 for the RRBP1 KO cell line) were imaged at 8 000 x nominal magnification with a pixel size of 1.4 nm. Images were contrast normalized and converted to 8-bit using Microscopy Image Browser (MIB, (Belevich et al., 2016)). For unbiased analysis, the images

were anonymized before manually segmenting peroxisomes and ER using MIB. The contact sites were analyzed using the MCcalc plug-in (Lak et al., 2021) in MIB software with probing distance of 150 nm, smoothing 15 and accepting gaps of 7 pixels. The peroxisomal area (peroxisomal size) and eccentricity (peroxisomal shape) were analyzed by MIB software (Belevich et al., 2016).

Statistical Analysis

All data are presented as mean ± standard deviation (SD). For the statistical analyses with two samples, student's unpaired two-tailed t-tests was performed using Graph Pad Prism Software. All the graphs and heat maps were prepared with Graph Pad Prism Software.

Funding

This work was supported by the European Research Council Starting Grant (grant nr. 637649 to Cory Dunn), Academy of Finland (grant nr. 331556 to Cory Dunn), Jane ja Aatos Erkon Säätiö (grant nr. 200057 to Cory Dunn), Sigrid Jusèlius Foundation (to Cory Dunn), Finnish Cultural Foundation (to KF) and financial support for thesis completion from the University of Helsinki Doctoral School (to KF).

Data availability

Full uncropped blot images are presented in Blot transparency file.

ACKNOWLEDGEMENTS

We thank the HiLife Flow Cytometry Unit at the University of Helsinki and Tiina Pessa-Morikawa for FACS service. Proteomics Unit at the Institute of Biotechnology, University of Helsinki, is acknowledged for mass spectrometry analysis of proteins. The Light Microscopy Unit of the Institute of Biotechnology at the University of Helsinki and Marko Crivaro are acknowledged for providing confocal microscopy service. Taina Suntio in the Electron Microscopy Unit (supported by HiLIFE and Biocenter Finland) at the Institute of Biotechnology, University of Helsinki, is acknowledged for EM sample preparation. We are grateful to Maria Vartiainen, Ville Hietakangas, Hien Bui, and Parijat Biswas for valuable discussions and suggestions. We also thank Xiang Le Chua for experimental support and Emilia Kuuluvainen, Leonardo Almeida-Souza, and Laura Hakanpää for their comments on the manuscript.

AUTHOR CONTRIBUTIONS

KF designed and performed experiments, analyzed data, wrote the manuscript. HV and EJ performed EM studies. BAA, AP and TS performed experiments. PK and VP discussed the project and commented on the manuscript. SK conceptualized and supervised the project, designed and performed experiments, analyzed data, wrote the manuscript. All authors commented on the manuscript.

CONFLICT OF INTEREST STATEMENT

The authors declare that they have no conflict of interest.

REFERENCES

Akşit, A., and I.J. van der Klei. 2018. Yeast peroxisomes: How are they formed and how do they grow? *Int J Biochem Cell Biol*. 105:24–34. doi:10.1016/J.BIOCEL.2018.09.019.

Albertini, M., P. Rehling, R. Erdmann, W. Girzalsky, J.A.K.W. Kiel, M. Veenhuis, and W.H. Kunau. 1997. Pex14p, a peroxisomal membrane protein binding both receptors of the two PTS-dependent import pathways. *Cell*. 89:83–92. doi:10.1016/S0092-8674(00)80185-3.

Anastasia, I., N. Ilacqua, A. Raimondi, P. Lemieux, R. Ghandehari-Alavijeh, G. Faure, S.L. Mekhedov, K.J. Williams, F. Caicci, G. Valle, M. Giacomello, A.D. Quiroga, R. Lehner, M.J. Miksis, K. Toth, T.Q. de Aguiar Vallim, E. V. Koonin, L. Scorrano, and L. Pellegrini. 2021. Mitochondria-rough-ER contacts in the liver regulate systemic lipid homeostasis. *Cell Rep*. 34. doi:10.1016/J.CELREP.2021.108873/ATTACHMENT/C935BB5D-0203-4599-9051-7D9ADFF4B483/MMC7.XLSX.

Aranovich, A., R. Hua, A.D. Rutenberg, and P.K. Kim. 2014. PEX16 contributes to peroxisome maintenance by constantly trafficking PEX3 via the ER. *J Cell Sci*. 127:3675–3686. doi:10.1242/jcs.146282.

Balboa, D., J. Weltner, S. Eurola, R. Trokovic, K. Wartiovaara, and T. Otonkoski. 2015. Conditionally Stabilized dCas9 Activator for Controlling Gene Expression in Human Cell Reprogramming and Differentiation. *Stem Cell Reports*. 5:448–459. doi:10.1016/J.STEMCR.2015.08.001.

Baldwin, H.A., C. Wang, G. Kanfer, H. V. Shah, A. Velayos-Baeza, M. Dulovic-Mahlow, N. Brüggemann, A. Anding, E. Baehrecke, D. Maric, W.A. Prinz, and R.J. Youle. 2021. VPS13D promotes peroxisome biogenesis. *J Cell Biol*. 220. doi:10.1083/JCB.202001188.

Belevich, I., M. Joensuu, D. Kumar, H. Vihinen, and E. Jokitalo. 2016. Microscopy Image Browser: A Platform for Segmentation and Analysis of Multidimensional Datasets. *PLoS Biol*. 14:e1002340. doi:10.1371/JOURNAL.PBIO.1002340.

Cardoen, B., K.R. Vandevoorde, G. Gao, M. Ortiz-Silva, P. Alan, W. Liu, E. Tiliakou, A.W. Vogl, G. Hamarneh, and I.R. Nabi. 2024. Membrane contact site detection (MCS-DETECT) reveals dual control of rough mitochondria-ER contacts. *J Cell Biol*. 223. doi:10.1083/JCB.202206109/VIDEO-9.

Costello, J.L., I.G. Castro, C. Hacker, T.A. Schrader, J. Metz, D. Zeuschner, A.S. Azadi, L.F. Godinho, V. Costina, P. Findeisen, A. Manner, M. Islinger, and M. Schrader. 2017. ACBD5 and VAPB mediate membrane associations between peroxisomes and the ER. *Journal of Cell Biology*. 216:331–342. doi:10.1083/JCB.201607055/VIDEO-2.

Cui, X.A., and A.F. Palazzo. 2014. Localization of mRNAs to the endoplasmic reticulum. *Wiley Interdiscip Rev RNA*. 5:481–492. doi:10.1002/WRNA.1225,.

Cui, X.A., H. Zhang, and A.F. Palazzo. 2012. P180 promotes the ribosome-independent localization of a subset of mRNA to the endoplasmic reticulum. *PLoS Biol*. 10. doi:10.1371/JOURNAL.PBIO.1001336,.

Dahan, N., Y.S. Bykov, E.A. Boydston, A. Fadel, Z. Gazi, H. Hochberg-Laufer, J. Martenson, V. Denic, Y. Shav-Tal, J.S. Weissman, N. Aviram, E. Zalckvar, and M. Schuldiner. 2022.

Peroxisome function relies on organelle-associated mRNA translation. *Sci Adv*. 8. doi:10.1126/SCIADV.ABK2141.

Demers, N.D., V. Riccio, D.S. Jo, S. Bhandari, K.B. Law, W. Liao, C. Kim, G.A. McQuibban, S.K. Choe, D.H. Cho, and P.K. Kim. 2023. PEX13 prevents pexophagy by regulating ubiquitinated PEX5 and peroxisomal ROS. *Autophagy*. 19:1781–1802. doi:10.1080/15548627.2022.2160566.

Distel, B., R. Erdmann, S.J. Gould, G. Blobel, D.I. Crane, J.M. Cregg, G. Dodt, Y. Fujiki, J.M. Goodman, W.W. Just, J.A.K.W. Kiel, W.H. Kunau, P.B. Lazarow, G.P. Mannaerts, H.W. Moser, T. Osumi, R.A. Rachubinski, A. Roscher, S. Subramani, H.F. Tabak, T. Tsukamoto, D. Valle, I. Van Der Klei, P.P. Van Veldhoven, and M. Veenhuis. 1996. A unified nomenclature for peroxisome biogenesis factors. *Journal of Cell Biology*. 135:1–3. doi:10.1083/JCB.135.1.1.

Erdmann, R., M. Veenhuis, D. Mertens, and W.H. Kunau. 1989. Isolation of peroxisome-deficient mutants of Saccharomyces cerevisiae. *Proceedings of the National Academy of Sciences*. 86:5419–5423. doi:10.1073/PNAS.86.14.5419.

Fang, Y., J.C. Morrell, J.M. Jones, and S.J. Gould. 2004. PEX3 functions as a PEX19 docking factor in the import of class I peroxisomal membrane proteins. *Journal of Cell Biology*. 164:863–875. doi:10.1083/JCB.200311131.

Farré, J., S.S. Mahalingam, M. Proietto, and S. Subramani. 2019. Peroxisome biogenesis, membrane contact sites, and quality control. *EMBO Rep*. 20. doi:10.15252/EMBR.201846864/ASSET/22FAEE4A-F7EA-41D5-B3C9-112000AD0BA8/ASSETS/GRAPHIC/EMBR201846864-FIG-0005-M.PNG.

Fujiki, Y., K. Okumoto, S. Mukai, M. Honsho, and S. Tamura. 2014. Peroxisome biogenesis in mammalian cells. *Front Physiol*. 5 AUG:102311. doi:10.3389/FPHYS.2014.00307/BIBTEX.

Germain, K., and P.K. Kim. 2020. Pexophagy: A Model for Selective Autophagy. *Int J Mol Sci*. 21. doi:10.3390/IJMS21020578.

Geuze, H.J., J.L. Murk, A.K. Stroobants, J.M. Griffith, M.J. Kleijmeer, A.J. Koster, A.J. Verkleij, B. Distel, and H.F. Tabak. 2003. Involvement of the endoplasmic reticulum in peroxisome formation. *Mol Biol Cell*. 14:2900–2907. doi:10.1091/MBC.E02-11-0734.

Goldman, B.M., and G. Blobel. 1978. Biogenesis of peroxisomes: intracellular site of synthesis of catalase and uricase. *Proc Natl Acad Sci U S A*. 75:5066–5070. doi:10.1073/PNAS.75.10.5066.

Guillén-Samander, A., M. Leonzino, M.G. Hanna, N. Tang, H. Shen, and P. De Camilli. 2021. VPS13D bridges the ER to mitochondria and peroxisomes via Miro. *J Cell Biol*. 220. doi:10.1083/JCB.202010004.

Haimovich, G., O. Cohen-Zontag, and J.E. Gerst. 2016. A role for mRNA trafficking and localized translation in peroxisome biogenesis and function? *Biochimica et Biophysica Acta (BBA) - Molecular Cell Research*. 1863:911–921. doi:10.1016/J.BBAMCR.2015.09.007.

Hasan, S., H.W. Platta, and R. Erdmann. 2013. Import of proteins into the peroxisomal matrix. *Front Physiol*. 4. doi:10.3389/FPHYS.2013.00261.

Hua, R., D. Cheng, É. Coyaud, S. Freeman, E. Di Pietro, Y. Wang, A. Vissa, C.M. Yip, G.D. Fairn, N. Braverman, J.H. Brumell, W.S. Trimble, B. Raught, and P.K. Kim. 2017. VAPs and

ACBD5 tether peroxisomes to the ER for peroxisome maintenance and lipid homeostasis. *Journal of Cell Biology*. 216:367–377. doi:10.1083/JCB.201608128.

Hung, V., S.S. Lam, N.D. Udeshi, T. Svinkina, G. Guzman, V.K. Mootha, S.A. Carr, and A.Y. Ting. 2017. Proteomic mapping of cytosol-facing outer mitochondrial and ER membranes in living human cells by proximity biotinylation. *Elife*. 6. doi:10.7554/ELIFE.24463.

Hung, V., N.D. Udeshi, S.S. Lam, K.H. Loh, K.J. Cox, K. Pedram, S.A. Carr, and A.Y. Ting. 2016. Spatially resolved proteomic mapping in living cells with the engineered peroxidase APEX2. *Nature Protocols 2016 11:3*. 11:456–475. doi:10.1038/nprot.2016.018.

Jokitalo, E., N. Cabrera-Poch, G. Warren, and D.T. Shima. 2001. Golgi clusters and vesicles mediate mitotic inheritance independently of the endoplasmic reticulum. *J Cell Biol*. 154:317. doi:10.1083/JCB.200104073.

Killackey, S.A., Y. Bi, D.J. Philpott, D. Arnoult, and S.E. Girardin. 2023. Mitochondria-ER cooperation: NLRX1 detects mitochondrial protein import stress and promotes mitophagy through the ER protein RRBP1. *Autophagy*. 19:1601. doi:10.1080/15548627.2022.2129763.

Kim, P.K., R.T. Mullen, U. Schumann, and J. Lippincott-Schwartz. 2006. The origin and maintenance of mammalian peroxisomes involves a de novo PEX16-dependent pathway from the ER. *Journal of Cell Biology*. 173:521–532. doi:10.1083/JCB.200601036.

Klouwer, F.C.C., K.D. Falkenberg, R. Ofman, J. Koster, D. van Gent, S. Ferdinandusse, R.J.A. Wanders, and H.R. Waterham. 2021. Autophagy Inhibitors Do Not Restore Peroxisomal Functions in Cells With the Most Common Peroxisome Biogenesis Defect. *Front Cell Dev Biol*. 9:661298. doi:10.3389/FCELL.2021.661298/BIBTEX.

Konovalova, S., X. Liu, P. Manjunath, S. Baral, N. Neupane, T. Hilander, Y. Yang, D. Balboa, M. Terzioglu, L. Euro, M. Varjosalo, and H. Tyynismaa. 2018. Redox regulation of GRPEL2 nucleotide exchange factor for mitochondrial HSP70 chaperone. *Redox Biol*. 19:37. doi:10.1016/J.REDOX.2018.07.024.

Konovalova, S., R. Torregrosa-Muñumer, P. Manjunath, X. Liu, S. Baral, K. Fatima, M. Holopainen, J. Kvist, J. Rajendran, Y. Yang, M. Varjosalo, R. Käkelä, P. Somerharju, and H. Tyynismaa. 2023. Small mitochondrial protein NERCLIN regulates cardiolipin homeostasis and mitochondrial ultrastructure. *Proc Natl Acad Sci U S A*. 120. doi:10.1073/PNAS.2210599120/-/DCSUPPLEMENTAL.

Koppers, M., N. Özkan, H.H. Nguyen, D. Jurriens, J. McCaughey, D.T.M. Nguyen, C.H. Li, R. Stucchi, M. Altelaar, H.D. MacGillavry, L.C. Kapitein, C.C. Hoogenraad, and G.G. Farías. 2024. Axonal endoplasmic reticulum tubules control local translation via P180/RRBP1-mediated ribosome interactions. *Dev Cell*. 59:2053-2068.e9. doi:10.1016/J.DEVCEL.2024.05.005.

Kurochkin, I. V., Y. Mizuno, A. Konagaya, Y. Sakaki, C. Schönbach, and Y. Okazaki. 2007. Novel peroxisomal protease Tysnd1 processes PTS1- and PTS2-containing enzymes involved in β-oxidation of fatty acids. *EMBO J*. 26:835. doi:10.1038/SJ.EMBOJ.7601525.

Lak, B., S. Li, I. Belevich, S. Sree, R. Butkovic, E. Ikonen, and E. Jokitalo. 2021. Specific subdomain localization of ER resident proteins and membrane contact sites resolved by electron microscopy. *Eur J Cell Biol*. 100:151180. doi:10.1016/J.EJCB.2021.151180.

Lam, S.K., N. Yoda, and R. Schekman. 2010. A vesicle carrier that mediates peroxisome protein traffic from the endoplasmic reticulum. doi:10.1073/pnas.1013397107.

Lam, S.S., J.D. Martell, K.J. Kamer, T.J. Deerinck, M.H. Ellisman, V.K. Mootha, and A.Y. Ting. 2014. Directed evolution of APEX2 for electron microscopy and proximity labeling. *Nature Methods 2014 12:1*. 12:51–54. doi:10.1038/nmeth.3179.

Lam, S.S., J.D. Martell, K.J. Kamer, T.J. Deerinck, M.H. Ellisman, V.K. Mootha, and A.Y. Ting. 2015. Directed evolution of APEX2 for electron microscopy and proximity labeling. *Nat Methods*. 12:51–54. doi:10.1038/NMETH.3179.

Liu, X., K. Salokas, F. Tamene, Y. Jiu, R.G. Weldatsadik, T. Öhman, and M. Varjosalo. 2018. An AP-MS- and BioID-compatible MAC-tag enables comprehensive mapping of protein interactions and subcellular localizations. *Nat Commun*. 9. doi:10.1038/S41467-018-03523-2.

Martell, J.D., T.J. Deerinck, S.S. Lam, M.H. Ellisman, and A.Y. Ting. 2017. Electron microscopy using the genetically encoded APEX2 tag in cultured mammalian cells. *Nat Protoc*. 12:1792. doi:10.1038/NPROT.2017.065.

Matsumoto, N., S. Tamura, and Y. Fujiki. 2003. The pathogenic peroxin Pex26p recruits the Pex1p-Pex6p AAA ATPase complexes to peroxisomes. *Nat Cell Biol*. 5:454–460. doi:10.1038/NCB982.

Miura, S., M. Mori, M. Takiguchi, M. Tatibana, S. Furuta, S. Miyazawa, and T. Hashimoto. 1984. THE JOURNAL OF BIOLOGICAL CHEMISTRY Biosynthesis and Intracellular Transport of Enzymes of Peroxisomal @-Oxidation*. 259. doi:10.1016/S0021-9258(20)82155-3.

Ogawa-Goto, K., K. Tanaka, T. Ueno, K. Tanaka, T. Kurata, T. Sata, and S. Irie. 2007. p180 Is Involved in the Interaction between the Endoplasmic Reticulum and Microtubules through a Novel Microtubule-binding and Bundling Domain. *Mol Biol Cell*. 18:3741. doi:10.1091/MBC.E06-12-1125.

Okumoto, K., N. Miyata, and Y. Fujiki. 2018. Identification of peroxisomal protein complexes with PTS receptors, pex5 and pex7, in mammalian cells. *Subcell Biochem*. 89:287–298. doi:10.1007/978-981-13-2233-4_12/FIGURES/4.

Rachubinski, R.A., Y. Fujiki, R.M. Mortensen, and P.B. Lazarow. 1984. Acyl-Coa oxidase and hydratase-dehydrogenase, two enzymes of the peroxisomal beta-oxidation system, are synthesized on free polysomes of clofibrate-treated rat liver. *Journal of Cell Biology*. 99:2241–2246. doi:10.1083/JCB.99.6.2241.

Rae, J., C. Ferguson, N. Ariotti, R.I. Webb, H.H. Cheng, J.L. Mead, J.D. Riches, D.J.B. Hunter, N. Martel, J. Baltos, A. Christopoulos, N.S. Bryce, M.L. Cagigas, S. Fonseka, M.E. Sayre, E.C. Hardeman, P.W. Gunning, Y. Gambin, T.E. Hall, and R.G. Parton. 2021. A robust method for particulate detection of a genetic tag for 3D electron microscopy. *Elife*. 10. doi:10.7554/ELIFE.64630.

Ran, F.A., P.D. Hsu, J. Wright, V. Agarwala, D.A. Scott, and F. Zhang. 2013. Genome engineering using the CRISPR-Cas9 system. *Nat Protoc*. 8:2281. doi:10.1038/NPROT.2013.143.

Ray, G.J., E.A. Boydston, E. Shortt, G.A. Wyant, S. Lourido, W.W. Chen, and D.M. Sabatini. 2020. A PEROXO-Tag Enables Rapid Isolation of Peroxisomes from Human Cells. *iScience*. 23:101109. doi:10.1016/J.ISCI.2020.101109.

Rubinson, D.A., C.P. Dillon, A. V. Kwiatkowski, C. Sievers, L. Yang, J. Kopinja, M. Zhang, M.T. McManus, F.B. Gertler, M.L. Scott, and L. Van Parijs. 2003. A lentivirus-based system to functionally silence genes in primary mammalian cells, stem cells and transgenic mice by RNA interference. *Nat Genet*. 33:401–406. doi:10.1038/NG1117.

Sakai, Y., M. Oku, I.J. van der Klei, and J.A.K.W. Kiel. 2006. Pexophagy: Autophagic degradation of peroxisomes. *Biochimica et Biophysica Acta (BBA) - Molecular Cell Research*. 1763:1767–1775. doi:10.1016/J.BBAMCR.2006.08.023.

Savitz, A.J., and D.I. Meyer. 1990. Identification of a ribosome receptor in the rough endoplasmic reticulum. *Nature 1990 346:6284*. 346:540–544. doi:10.1038/346540a0.

Schliebs, W., J. Saidowsky, B. Agianian, G. Dodt, F.W. Herberg, and W.-H. Kunau. 1999. Recombinant Human Peroxisomal Targeting Signal Receptor PEX5. *Journal of Biological Chemistry*. 274:5666–5673. doi:10.1074/jbc.274.9.5666.

Schmid-Burgk, J.L., K. Höning, T.S. Ebert, and V. Hornung. 2016. CRISPaint allows modular base-specific gene tagging using a ligase-4-dependent mechanism. *Nat Commun*. 7. doi:10.1038/NCOMMS12338.

Schmidt, E.K., G. Clavarino, M. Ceppi, and P. Pierre. 2009. SUnSET, a nonradioactive method to monitor protein synthesis. *Nature Methods 2009 6:4*. 6:275–277. doi:10.1038/nmeth.1314.

Schmidt, F., D. Dietrich, R. Eylenstein, Y. Groemping, T. Stehle, and G. Dodt. 2012. The role of conserved PEX3 regions in PEX19-binding and peroxisome biogenesis. *Traffic*. 13:1244–1260. doi:10.1111/J.1600-0854.2012.01380.X.

Sengupta, R., M.J. Poderycki, and S. Mattoo. 2019. CryoAPEX - an electron tomography tool for subcellular localization of membrane proteins. *J Cell Sci*. 132. doi:10.1242/JCS.222315/VIDEO-2.

Shibata, Y., T. Shemesh, W.A. Prinz, A.F. Palazzo, M.M. Kozlov, and T.A. Rapoport. 2010. Mechanisms determining the morphology of the peripheral ER. *Cell*. 143:774. doi:10.1016/J.CELL.2010.11.007.

Somborac, T., G. Lutfullahoglu Bal, K. Fatima, H. Vihinen, A. Paatero, E. Jokitalo, V.O. Paavilainen, and S. Konovalova. 2023. The subset of peroxisomal tail-anchored proteins do not reach peroxisomes via ER, instead mitochondria can be involved. *PLoS One*. 18:e0295047. doi:10.1371/JOURNAL.PONE.0295047.

Sugiura, A., S. Mattie, J. Prudent, and H.M. Mcbride. 2017. Newly born peroxisomes are a hybrid of mitochondrial and ER-derived pre-peroxisomes. *Nature*. 542:251–254. doi:10.1038/NATURE21375;SUBJMETA.

Walter, T., and R. Erdmann. 2019. Current Advances in Protein Import into Peroxisomes. *Protein J*. 38:351–362. doi:10.1007/S10930-019-09835-6.

Van Der Zand, A., I. Braakman, and H.F. Tabak. 2010. Peroxisomal Membrane Proteins Insert into the Endoplasmic Reticulum. *Mol Biol Cell*. 21:2057. doi:10.1091/MBC.E10-02-0082.

Zipor, G., L. Haim-Vilmovsky, R. Gelin-Licht, N. Gadir, C. Brocard, and J.E. Gerst. 2009. Localization of mRNAs coding for peroxisomal proteins in the yeast, Saccharomyces cerevisiae. *Proc Natl Acad Sci U S A*. 106:19848–19853. doi:10.1073/PNAS.0910754106,.

FIGURE LEGENDS

Figure 1. Systematic identification of peroxisome biogenesis factors using proximity labeling and CRISPR/Cas9 microscopy-based screen.
(A) Overview of the APEX2-based proximity labeling approach to identify peroxisome biogenesis factors. (B) Filtering steps of mass spectrometry data to identify highly confident peroxisome biogenesis factors. (C) Overview of the CRISPR/Cas9 microscopy-based screen. (D) Heat map of CRISPR/Cas9 microscopy assessing the phenotype of HEK293T cells. HEK293T cells stably expressing GFP-APEX2-ePTS1 were transiently transfected with gRNAs and Cas9-mCherry plasmid as shown in (C). Two rounds of transfection were performed (I and II). Each round the phenotype of the cells was assessed three times at 7, 10 and 14 post-transfection days using live-cell fluorescence microscopy. Cells were manually classified based on GFP localization: “no” (GFP localized exclusively to peroxisomes, no mislocalization), “mild” (some mislocalized GFP), “strong” (substantial mislocalized GFP), and “very strong” (extensive mislocalized GFP). gRNAs targeting PEX5 or PEX19 were used as positive controls (in green). The full list of the screened gRNAs is in the Supplementary Figure 1. (E) Live-cell fluorescence microscopy images of HEK293T cells stably expressing GFP-APEX2-ePTS1 before and after 13 days of transfection with Cas9-mCherry plasmid and gRNA targeting RRBP1, PEX5 or PEX19. The localization of peroxisomal targeted construct GFP-APEX2-ePTS1 was visualized using green channel. Scale bar, 50 μm.

Figure 2. RRBP1 is required for normal peroxisome maintenance in human cells.
(A) Western blot analysis of RRBP1 KO HEK293T cells stably expressing GFP-APEX2-ePTS1. Parental, PEX3 and PEX19 KO HEK293T cells not expressing peroxisomal targeted construct were used as controls. GAPDH was used as a loading control. (B) Quantification of peroxisomal protein levels using western blot images represented in (A) (n = 3-4). (C) Quantification of ACOX1 processing using western blot images represented in (A) (n = 3-4). (D) Quantification of ER protein levels using western blot images represented in (A) (n = 3-5). (E) Quantification of TOM20 protein level using western blot images represented in (A) (n = 3-4). Each western blot analysis was performed at least three times. Values are normalized to the corresponding parental cell line, set to 1. In all graphs data are presented as mean ± SD. *P <0.05, **P < 0.01, ***P < 0.001, ****P < 0.0001, ns, not significant as compared to the parental cell line (unpaired t-tests).

Figure 3. RRBP1 silencing causes peroxisomal deficiency in human cells.
(A) Western blot analysis of RRBP1 silencing in HEK293T cells stably expressing GFP-APEX2-ePTS1. The cells were transfected with corresponding esiRNAs for 72 h. GFP esiRNA was used as a negative control, esiRNA PEX5 was used as a positive control. NT, non-treated cells. (B-D) Quantification of western blot images presented in (A) (n = 3 in (B) and (D), n = 4 in (C). GAPDH or tubulin was used as a loading controls. Each western blot analysis was performed at least three times. Values are normalized to the non-treated cells, set at 1. In all graphs data are presented as mean ± SD. *P < 0.05, **P < 0.01, ns, not significant (unpaired t-tests). (E) Live-cell fluorescence

microscopy images of cells HEK293T cells stably expressing GFP-APEX2-ePTS1 before and after transfection with indicated esiRNAs. The localization of peroxisomal targeted construct GFP-APEX2-ePTS1 was visualized using green channel. GFP esiRNA was used as a negative control, esiRNA PEX5 was used as a positive control. Scale bar, 25 μm. Images are representative of two independent transfection experiments.

Figure 4. The number of peroxisomes is decreased in RRBP1 KO cells.
(A) Confocal microscopy images of RRBP1 KO or parental HEK293T cells stably expressing GFP-APEX2-ePTS1. Immunostaining was performed using anti-PEX14, anti-GFP, anti-catalase or anti-RRBP1 antibody. Scale bar, 5 μm. (B) Confocal microscopy images of RRBP1 KO or parental HEK293T cells stably expressing GFP-APEX2-ePTS1. Immunostaining was performed using anti-PMP70 and anti-GFP antibody. Scale bar, 5 μm. (C-E) Quantification of PEX14-, PMP70-, or catalase-positive puncta in RRBP1 KO and parental HEK293T cells stably expressing GFP-APEX2-ePTS1. Z-stacks of confocal microscopy images were processed and reconstructed in 3D model with Imaris software. Each value represents analysis of around 100 cells. (F) The volume of RRBP1 KO or parental HEK293T cells stably expressing GFP-APEX2-ePTS1 was analyzed using confocal microscopy images. Z-stacks of confocal microscopy images were processed and reconstructed in 3D model with Imaris software. Immunostaining for each protein was performed in at least three independent experiments. Each value represents analysis of around 100 cells. PEX14 or catalase signal was used for the analysis. In all graphs data are presented as mean ± SD. $^{**}P < 0.01$, $^{***}P < 0.001$, ns, not significant as compared to the parental cell line (unpaired t-tests).

Figure 5. RRBP1 does not localize to peroxisomes.
(A) Intracellular localization of RRBP1 was analyzed in HEK293T cells using immunofluorescence confocal microscopy. Catalase was used to label peroxisomes, ATPIF1was used to visualize mitochondria, calnexin was used to label ER. Scale bar, 3 μm. Immunostaining for each protein was performed in at least three independent experiments. (B) Colocalization analysis of confocal microscopy images represented in (A) by Mander's overlap coefficient. The data are presented as mean ± SD. Immunostaining for each protein was performed in at least three independent experiments. (C) Western blot of HEK293T cells stably expressing 3×HA-EGFP-PEX26 (HA-PEROXO) and immunopurified peroxisomes. Each western blot analysis was performed at least two times.

Figure 6. Peroxisome-ER contact sites are not affected in RRBP1-depleted cells.
(A) Representative electron microscopy images of RRBP1 KO or parental HEK293T cells stably expressing GFP-APEX2-ePTS1. Peroxisomes were labeled by DAB staining. Scale bar, 200 nm. PO, peroxisome; ER, endoplasmic reticulum. Experiments were performed in at least two independent replicates for each cell line and condition. (B) Representative electron microscopy images of non-transfected HEK293T cells stability expressing GFP-APEX2-ePTS1 or cells transfected for 48 h with esiRNAs targeting RRBP1 or luciferase (Luc) as a negative control. Peroxisomes were labeled by DAB staining. Scale bar, 200 nm. PO, peroxisome; ER, endoplasmic reticulum. (C) Relative distribution of peroxisome-ER contact sites at 10 – 100 nm distance in RRBP1 KO or parental HEK293T cells stability expressing GFP-APEX2-ePTS1 analyzed by electron microscopy images. In each experiment for each cell line 13-18 cells having peroxisomal profiles were selected using systematic random sampling. All the peroxisomes in the selected cells were imaged (n = 105 - 175 for each replicate of parental cell line, n = 84 - 168 for each replicate of RRBP1 KO cell line) and the peroxisomal-ER distances were analyzed using Microscopy Image

Browser (MIB, (Belevich et al., 2016)). (D) Relative distribution of peroxisome-ER contact sites at 10 – 100 nm distance in non-transfected HEK293T cells stability expressing GFP-APEX2-ePTS1 (NT) or in cells transfected for 48 h with esiRNAs targeting RRBP1 or lu-ciferase (Luc) as a negative control. (E) Western blot analysis of RRBP1 silencing in HEK293T cells stably expressing GFP-APEX2-ePTS1. The cells were transfected with corresponding esiRNAs for 24 or 48 h. Lu-ciferase (Luc) esiRNA was used as a negative control. Each western blot analysis was performed at least two times. (F) The distribution of the peroxisomal area (peroxiso-mal size) analyzed in RRBP1 KO (n = 437) or parental HEK293T cells (n = 403) stably expressing GFP-APEX2-ePTS1. Electron microscopy images and Microscopy Image Browser (MIB, (Belevich et al., 2016)) were used for the analysis. (G) Eccentricity (peroxisomal shape) was analyzed using electron microscopy images and Microscopy Image Browser (MIB, (Belevich et al., 2016). In all graphs data are presented as mean ± SD, ns, not significant as compared to the parental cell line (unpaired t-tests).

Figure 7. The decreased number of peroxisomes in RRBP1 KO cells is independent of pexophagy but associated with increased proteasomal degradation of peroxisomal membrane proteins.

(A) Western blot analysis of RRBP1 KO or parental HEK293T cells stability expressing GFP-APEX2-ePTS1 construct before and after treatment with 100 µM chloroquine for 3 h. GAPDH was used as a loading control. (B) Quantification of western blot images presented in (A) (n = 3). (C) Western blot analysis of RRBP1 KO or parental HEK293T cells stability expressing GFP-APEX2-ePTS1 construct before and after treatment with 10 µM MG132 for 4 h. Stain-Free total protein staining was used as a loading control. (D) Quantification of western blot images presented in (C) (n = 3). Each western blot analysis was performed at least two times. Values are normalized to the parental cell line, set to 1. In all graphs data are presented as mean ± SD. *P < 0.05, **P < 0.01, ***P < 0.001, ns, not significant (unpaired t-tests).

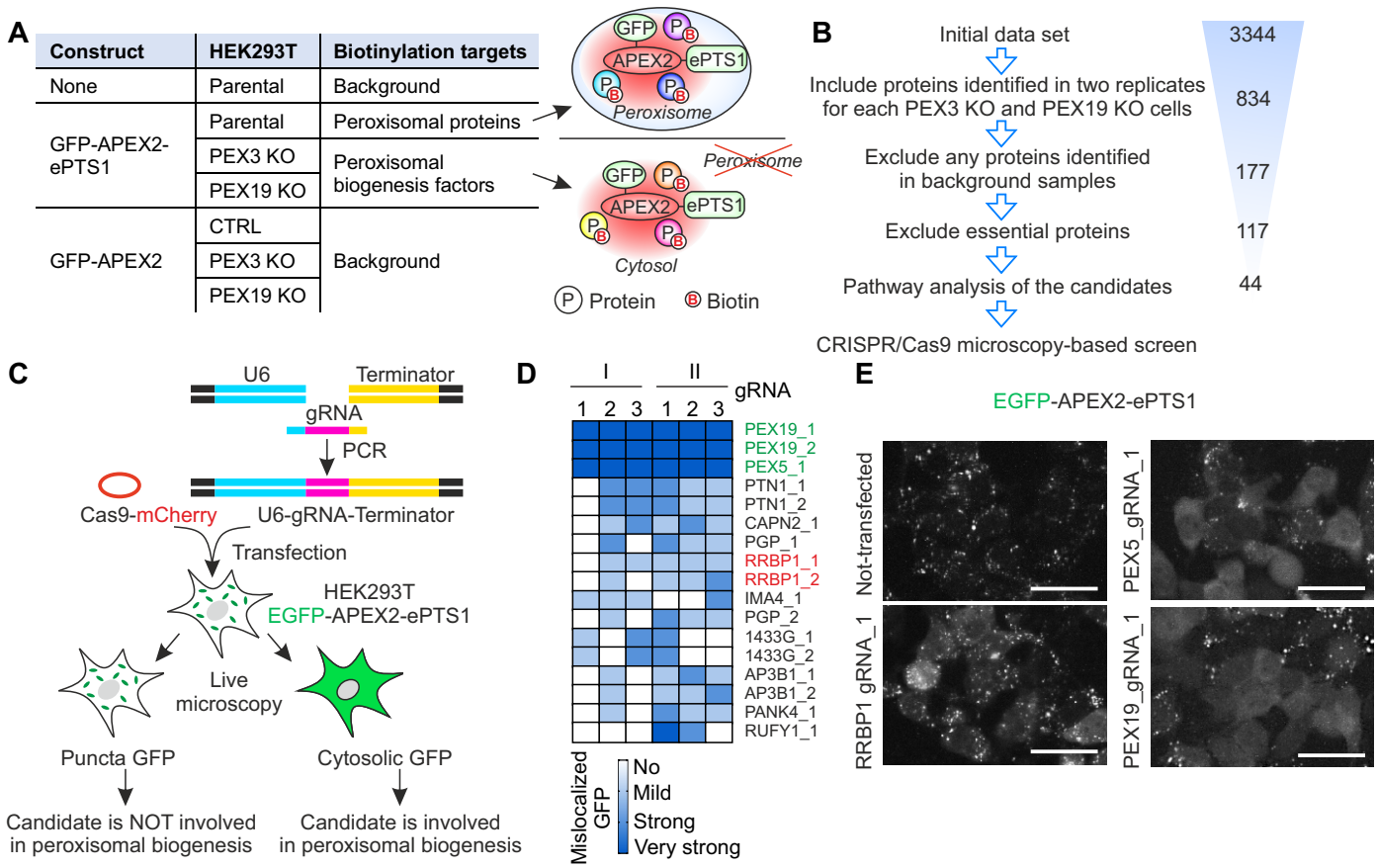
A
Construct
HEK293T
Biotinylation targets
None
Parental
Background
GFP-APEX2-ePTS1
Parental
Peroxisomal proteins
PEX3 KO
PEX19 KO
Peroxisomal biogenesis factors
GFP-APEX2
CTRL
PEX3 KO
PEX19 KO
Background
GFP
APEX2
ePTS1
Peroxisome
Cytosol
Protein
Biotin
B
Initial data set
3344
Include proteins identified in two replicates for each PEX3 KO and PEX19 KO cells
834
Exclude any proteins identified in background samples
177
Exclude essential proteins
117
Pathway analysis of the candidates
44
CRISPR/Cas9 microscopy-based screen
C
U6
Terminator
gRNA
PCR
Cas9-mCherry
U6-gRNA-Terminator
Transfection
HEK293T
EGFP-APEX2-ePTS1
Live microscopy
Puncta GFP
Cytosolic GFP
Candidate is NOT involved in peroxisomal biogenesis
Candidate is involved in peroxisomal biogenesis
D
I
II
gRNA
1 2 3 1 2 3
PEX19_1
PEX19_2
PEX5_1
PTN1_1
PTN1_2
CAPN2_1
PGP_1
RRBP1_1
RRBP1_2
IMA4_1
PGP_2
1433G_1
1433G_2
AP3B1_1
AP3B1_2
PANK4_1
RUFY1_1
Mislocalized GFP
No
Mild
Strong
Very strong
E
EGFP-APEX2-ePTS1
Not-transfected
PEX5_gRNA_1
RRBP1 gRNA_1
PEX19_gRNA_1

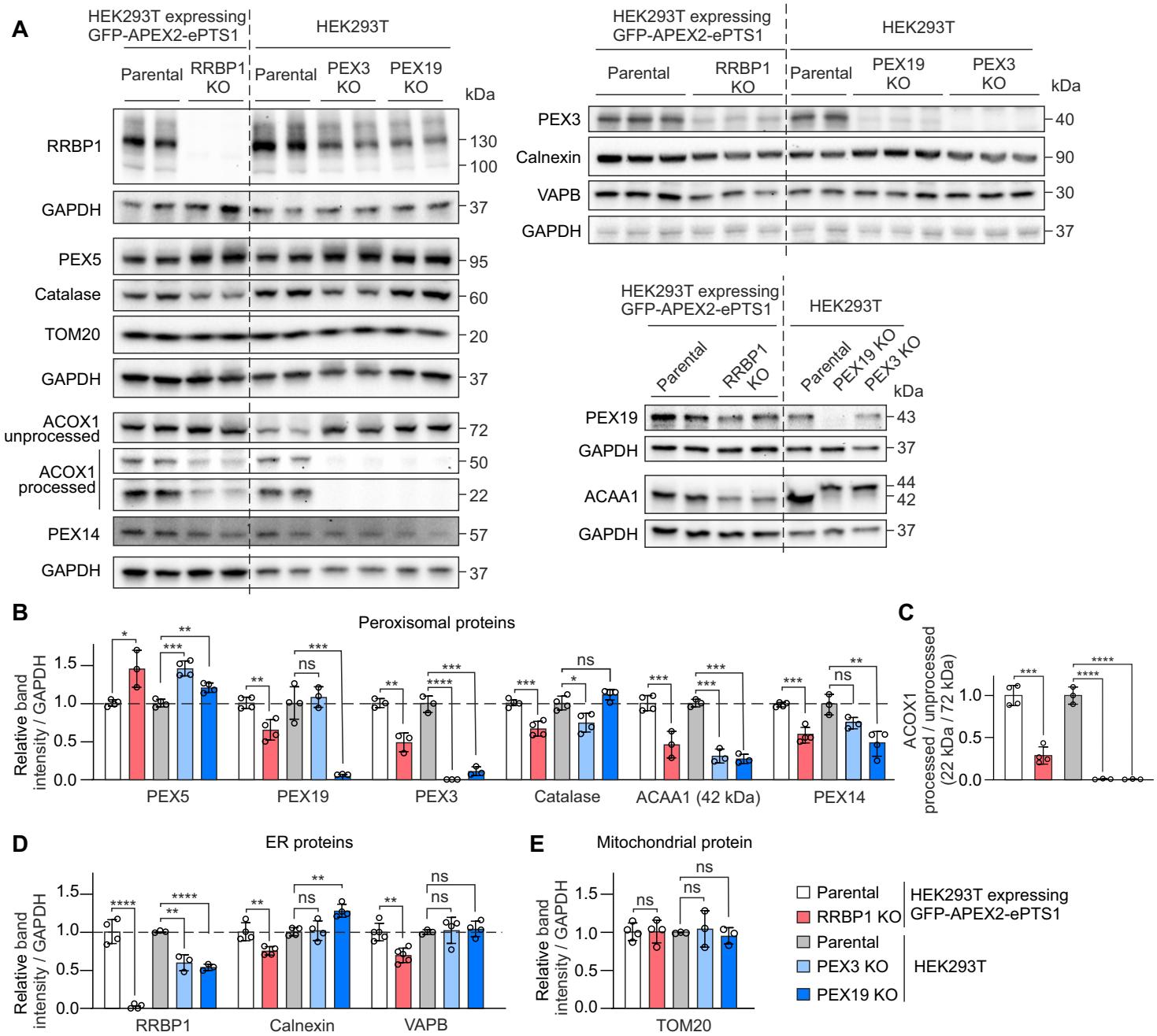
A
HEK293T expressing GFP-APEX2-ePTS1
HEK293T
Parental
RRBP1 KO
Parental
PEX3 KO
PEX19 KO
kDa
RRBP1
GAPDH
PEX5
Catalase
TOM20
GAPDH
ACOX1 unprocessed
ACOX1 processed
PEX14
GAPDH
130
100
37
95
60
20
37
72
50
22
57
37
PEX3
Calnexin
VAPB
GAPDH
40
90
30
37
PEX19
GAPDH
ACAA1
GAPDH
43
37
44
42
37
B
Peroxisomal proteins
Relative band intensity / GAPDH
PEX5
PEX19
PEX3
Catalase
ACAA1 (42 kDa)
PEX14
C
ACOX1 processed / unprocessed (22 kDa / 72 kDa)
D
ER proteins
RRBP1
Calnexin
VAPB
E
Mitochondrial protein
TOM20
Parental
RRBP1 KO
HEK293T expressing GFP-APEX2-ePTS1
Parental
PEX3 KO
PEX19 KO
HEK293T

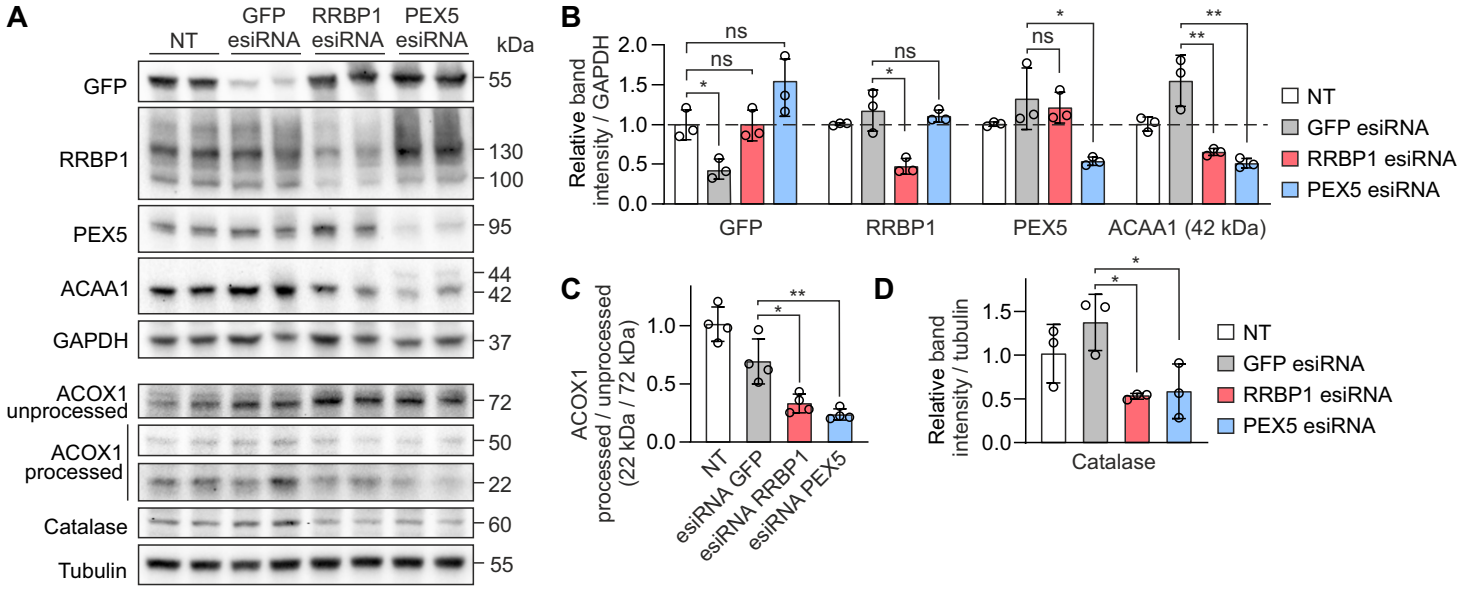
A
NT
GFP esiRNA
RRBP1 esiRNA
PEX5 esiRNA
kDa
GFP
RRBP1
PEX5
ACAA1
GAPDH
ACOX1 unprocessed
ACOX1 processed
Catalase
Tubulin
55
130
100
95
44
42
37
72
50
22
60
55
B
Relative band intensity / GAPDH
ns
*
**
GFP
RRBP1
PEX5
ACAA1 (42 kDa)
NT
GFP esiRNA
RRBP1 esiRNA
PEX5 esiRNA
C
ACOX1 processed / unprocessed (22 kDa / 72 kDa)
NT
esiRNA GFP
esiRNA RRBP1
esiRNA PEX5
D
Relative band intensity / tubulin
Catalase

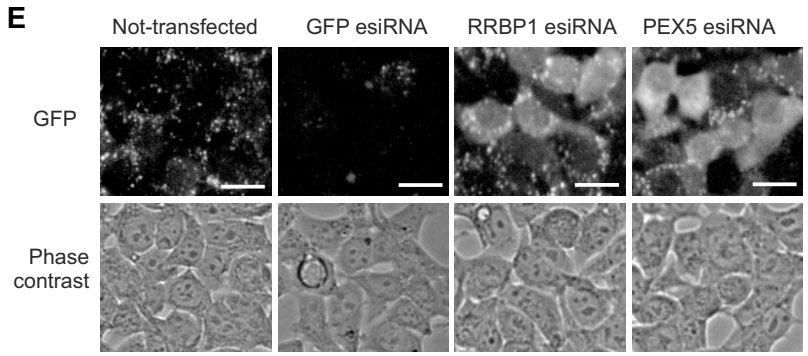
E
Not-transfected
GFP esiRNA
RRBP1 esiRNA
PEX5 esiRNA
GFP
Phase contrast

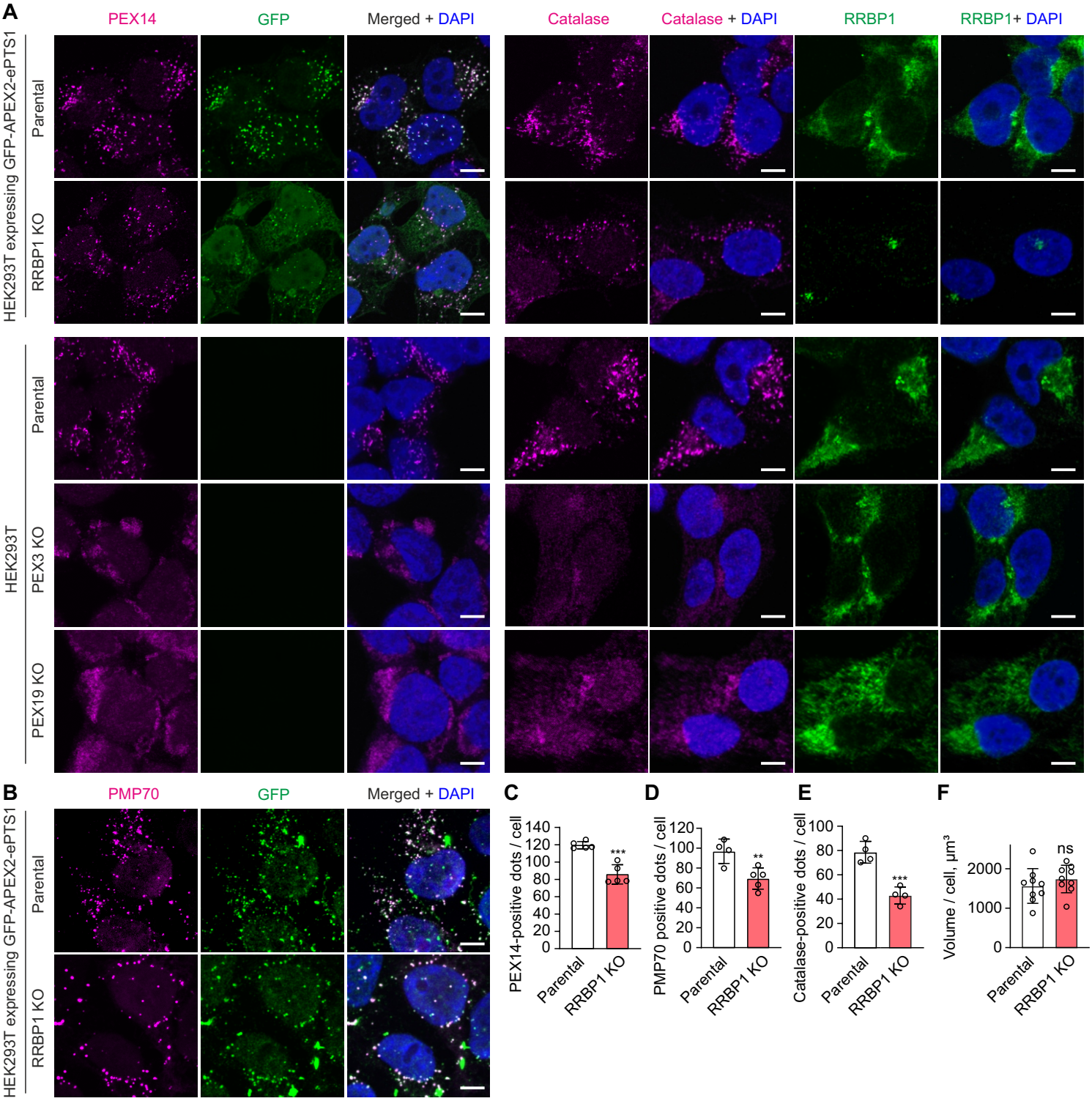
A
PEX14
GFP
Merged + DAPI
Catalase
Catalase + DAPI
RRBP1
RRBP1+ DAPI
HEK293T expressing GFP-APEX2-ePTS1
Parental
RRBP1 KO
HEK293T
Parental
PEX3 KO
PEX19 KO
B
PMP70
GFP
Merged + DAPI
HEK293T expressing GFP-APEX2-ePTS1
Parental
RRBP1 KO
C
PEX14-positive dots / cell
140
120
100
80
60
40
20
0
***
Parental
RRBP1 KO
D
PMP70 positive dots / cell
120
100
80
60
40
20
0
**
Parental
RRBP1 KO
E
Catalase-positive dots / cell
100
80
60
40
20
0
***
Parental
RRBP1 KO
F
Volume / cell, µm³
2000
1000
0
ns
Parental
RRBP1 KO

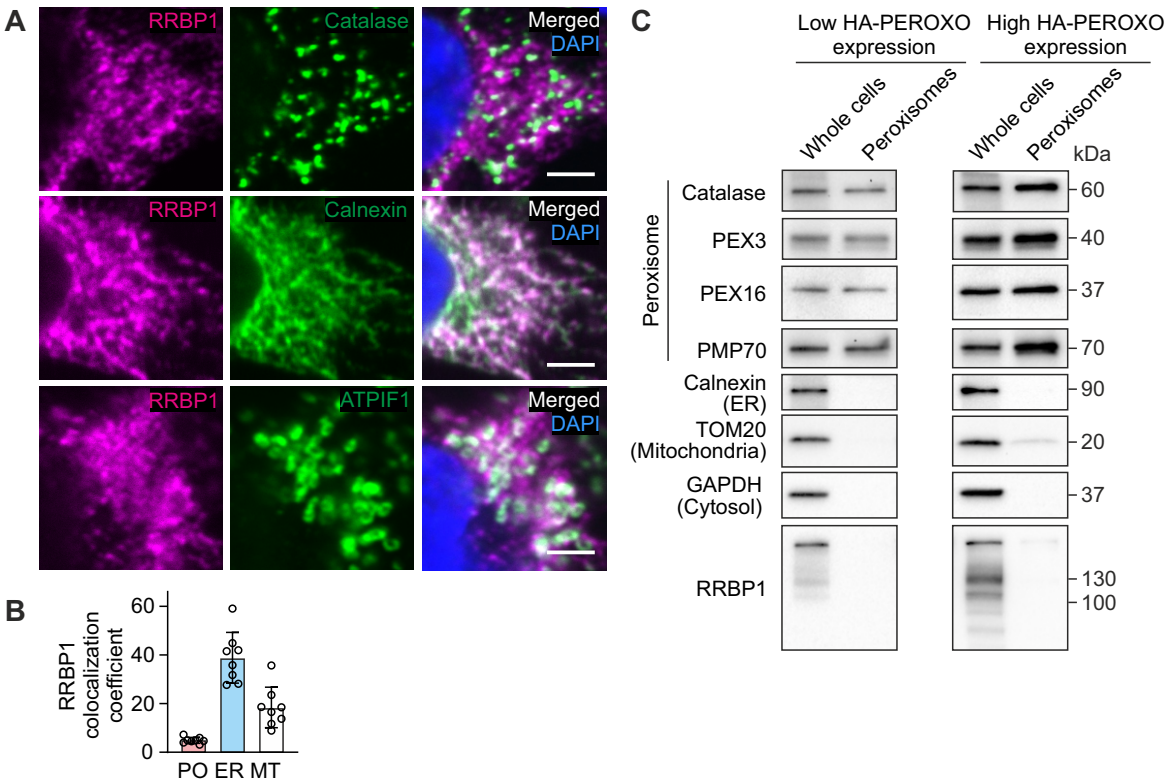
A
RRBP1
Catalase
Merged
DAPI
RRBP1
Calnexin
Merged
DAPI
RRBP1
ATPIF1
Merged
DAPI
B
RRBP1 colocalization coefficient
60
40
20
0
PO ER MT
C
Low HA-PEROXO expression
High HA-PEROXO expression
Whole cells
Peroxisomes
Whole cells
Peroxisomes
kDa
Peroxisome
Catalase
PEX3
PEX16
PMP70
Calnexin (ER)
TOM20 (Mitochondria)
GAPDH (Cytosol)
RRBP1
60
40
37
70
90
20
37
130
100

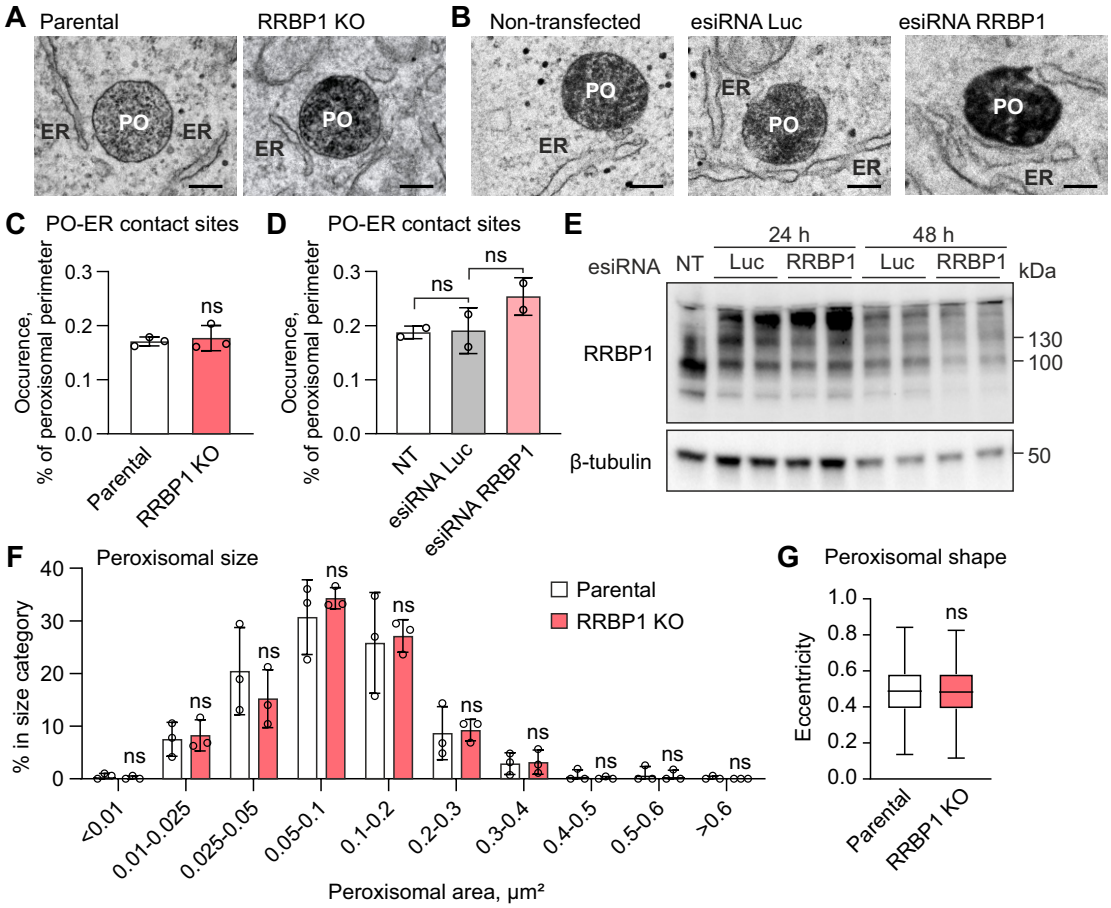
A
Parental
RRBP1 KO
ER
PO
ER
PO
ER
B
Non-transfected
esiRNA Luc
esiRNA RRBP1
PO
ER
ER
PO
ER
PO
ER
C
PO-ER contact sites
Occurence, % of peroxisomal perimeter
0.3
0.2
0.1
0.0
ns
Parental
RRBP1 KO
D
PO-ER contact sites
Occurence, % of peroxisomal perimeter
0.3
0.2
0.1
0.0
ns
ns
NT
esiRNA Luc
esiRNA RRBP1
E
24 h
48 h
esiRNA
NT
Luc
RRBP1
Luc
RRBP1
kDa
RRBP1
130
100
β-tubulin
50
F
Peroxisomal size
% in size category
40
30
20
10
0
Parental
RRBP1 KO
ns
<0.01
0.01-0.025
0.025-0.05
0.05-0.1
0.1-0.2
0.2-0.3
0.3-0.4
0.4-0.5
0.5-0.6
>0.6
Peroxisomal area, µm²
G
Peroxisomal shape
Eccentricity
1.0
0.8
0.6
0.4
0.2
0.0
ns
Parental
RRBP1 KO

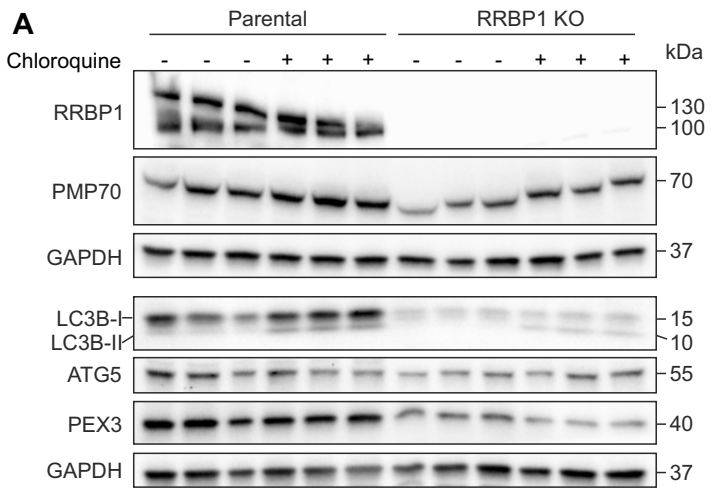
A
Parental
RRBP1 KO
Chloroquine
- - - + + + - - - + + +
kDa
RRBP1
PMP70
GAPDH
LC3B-I
LC3B-II
ATG5
PEX3
GAPDH
130
100
70
37
15
10
55
40
37

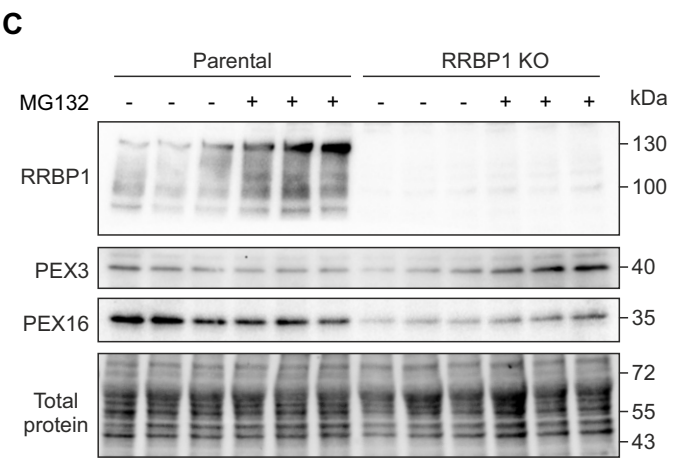
C
Parental
RRBP1 KO
MG132
- - - + + + - - - + + +
kDa
RRBP1
PEX3
PEX16
Total protein
130
100
40
35
72
55
43

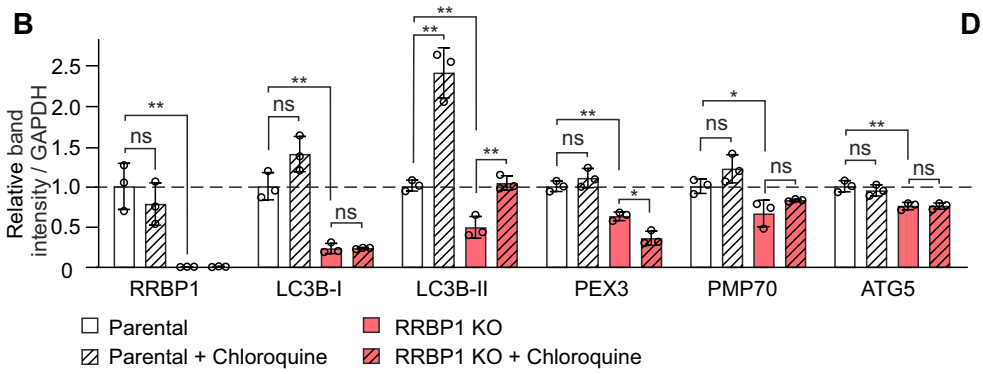
B
Relative band intensity / GAPDH
2.5
2.0
1.5
1.0
0.5
0
RRBP1
LC3B-I
LC3B-II
PEX3
PMP70
ATG5
ns
**
*
Parental
Parental + Chloroquine
RRBP1 KO
RRBP1 KO + Chloroquine

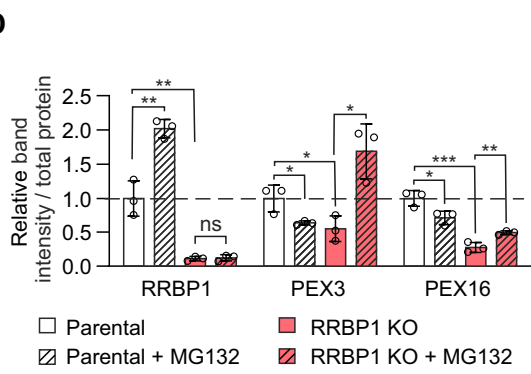
D
Relative band intensity / total protein
2.5
2.0
1.5
1.0
0.5
0.0
RRBP1
PEX3
PEX16
ns
*
**
***
Parental
Parental + MG132
RRBP1 KO
RRBP1 KO + MG132